Flavodiiron proteins and NDH-1 cooperate to maintain photosynthetic redox poise in *Synechocystis*

Lauri Nikkanen[1], Anita Santana Sánchez[1], Maria Ermakova[1*], Matthias Rögner[2], Laurent Cournac[3], and Yagut Allahverdiyeva[1#]

Affiliations:

[1]Molecular Plant Biology, Department of Biochemistry, University of Turku, Turku, Finland

[2]Plant Biochemistry, Faculty of Biology & Biotechnology, Ruhr-University Bochum, Bochum, Germany

[3]Eco&Sols, Univ Montpellier, IRD, CIRAD, INRA, Montpellier Supagro, Montpellier, France

[*]Current affiliation: Australian Research Council Centre of Excellence for Translational Photosynthesis, Division of Plant Science, Research School of Biology, The Australian National University, Acton, Australia

Correspondence: Yagut Allahverdiyeva allahve@utu.fi

Running title: *FDPs and NDH-1 cooperatively safeguard PSI*

ABSTRACT

In photosynthetic organisms apart from Angiosperms, flavodiiron proteins (FDPs) catalyze light-dependent reduction of O_2 to H_2O alleviating electron pressure on PSI and protecting it from photodamage. In *Synechocystis* sp. PCC 6803, four FDP isoforms function as hetero-oligomers of Flv1 and Flv3 and/or Flv2 and Flv4. The NAD(P)H dehydrogenase-like complex (NDH-1), in turn, is essential for C_i uptake, respiration and cyclic electron transfer. Four NDH-1 types haven been characterized in *Synechocystis*. NDH-1L and NDH-1L´ function in respiration and cyclic electron transfer, and NDH-1MS and NDH-1MS´ in CO_2 uptake. We have characterized triple mutants lacking Flv1 or Flv3 and the D1 and D2 subunits of NDH-1, resulting in deficiency of NDH-1L and NDH-1L´. Our results suggest functional redundancy and crosstalk between FDPs and NDH-1 under studied conditions. While ΔFlv1 or ΔFlv3 single mutants and ΔNdhD1/D2 double mutants can acclimate to a change of growth conditions from moderate light / high CO_2 to high light / low CO_2 and grow like wild-type cells, the ΔFlv1 (or Flv3)/NdhD1/D2 triple mutants are unable to survive the shift. Our results demonstrate that the functions of FDPs and NDH-1 are dynamically coordinated to allow efficient oxidation of PSI and photoprotection under variable light conditions and C_i availability.

KEYWORDS: photosynthesis; Synechocystis; Flavodiiron proteins; NDH-1; FDP; Flv; complex I; photoprotection; Mehler-like reaction, Mehler reaction, auxiliary electron transfer

INTRODUCTION

Photosynthetic organisms have evolved a variety of different regulatory mechanisms to protect the photosynthetic machinery during rapid changes in environmental conditions (Allahverdiyeva et al., 2015). It is particularly important to prevent over-reduction of the photosynthetic electron transport chain (PETC) in fluctuating light intensities, which would result in photodamage to the photosystems (Allahverdiyeva et al., 2015; Tiwari et al., 2016; Shimakawa et al., 2016). In plants apart from angiosperms, in algae, and especially in cyanobacteria, the essential mechanism to this end is the Mehler-like reaction catalyzed by C-type flavodiiron proteins (FDPs) (Allahverdiyeva et al., 2013; Gerotto et al., 2016; Ilik et al., 2017; Chaux et al., 2017; Jokel et al., 2018; Alboresi et al., 2019). The Mehler-like reaction involves photoreduction of O_2 using electrons derived from downstream of PSI, producing H_2O (Vicente et al., 2002; Brown et al., 2019). Importantly and in contrast to the Mehler reaction, FDPs do not produce harmful reactive oxygen species (ROS) (Vicente et al., 2002; Brown et al., 2019). The genome of the *β*-cyanobacterium *Synechocystis* sp. PCC 6803 (hereafter *Synechocystis*) encodes four isoforms of FDPs, namely Flv1-4, which function in O_2 photoreduction mainly as hetero-oligomers consisting of either Flv1 and Flv3 or Flv2 and Flv4 (Zhang et al., 2004; Mustila et al., 2016; Santana-Sanchez et al., 2019). Recently we showed that under air level [CO_2], Flv1/3 and Flv2/4 hetero-oligomers function in a coordinated manner: Flv1/3 catalyzes strong, transient O_2 photoreduction upon onset of illumination or during increases in light intensity, functioning as a strong sink for excessive electrons in the PETC, while Flv2/4 hetero-oligomers catalyze slower and limited steady state reduction of O_2, also using electrons downstream of PSI (Santana-Sanchez et al., 2019). In elevated [CO_2] and in air [CO_2] at alkaline pH 9, the *flv4-flv2* operon encoding Flv2, Flv4, and the Sll0218 protein is downregulated (Zhang et al., 2009; Santana-Sanchez et al., 2019). Nevertheless, a low level of Flv1/3 in elevated [CO_2] catalyzes steady state O_2 photoreduction, whereas in air [CO_2] at pH 9 is responsible for strong but transient O_2 photoreduction (Santana-Sanchez et al., 2019).

In cyanobacteria, photosynthetic and respiratory electron transfer reactions coexist on thylakoid membranes and are intricately intertwined, necessitating strict regulation (Mullineaux, 2014). The NADH dehydrogenase-like complex 1 (NDH-1, photosynthetic Complex I) is involved in several electron transfer pathways that allow acclimation to environmental changes. Depending on its subunit configuration, cyanobacterial NDH-1 functions in cyclic electron transfer around PSI (CET), respiration, and in CO_2 uptake in the carbon concentrating mechanism (CCM) (Ohkawa et al., 2000; Shibata et al., 2001; Zhang et al., 2004; Bernat et al., 2011; Burnap et al., 2013; Peltier et

al., 2016). The NDH-1L form features the subunits NdhD1 and NdhF1 and catalyzes both CET from ferredoxin (Fd) to plastoquinone (PQ) coupled to pumping of a $4H^+/2e^-$ into the thylakoid lumen, and functions as Complex I of the respiratory electron transfer chain (Zhang et al., 2004; He et al., 2015; Laughlin et al., 2019; Schuller et al., 2019; Saura and Kaila, 2019). The NDH-1L´ form features the NdhD2 instead of NdhD1 subunit, but it remains unclear whether NDH-1L and NDH-1L´ serve different physiological functions (Peltier et al., 2016). The NDH-1MS and NDH-1MS´ forms that comprise the subunits NdhD3, NdhF3, CupA, and CupS, or NdhD4, NdhF4, and CupB, respectively, function in conversion of CO_2 to HCO_3^- (Ohkawa et al., 2000; Zhang et al., 2004; Han et al., 2017; Schuller et al., 2019), possibly enabled by alkaline pockets at the thylakoid membrane created by NDH-1 proton pumping (Kaplan and Reinhold, 1999). NDH-1MS complexes can likely also catalyze CET, albeit to a lesser extent than NDH-1L (Bernat et al., 2011).

In the current study, we strive to elucidate how the electron transfer pathways mediated by FDPs and NDH-1L cooperate to allow maintenance of redox balance between the PETC, respiration, CCM, and CO_2 fixation in the Calvin-Benson cycle (CBC) during changes in light intensity and Ci availability. To this end, we used both biophysical and biochemical methods to characterize *Synechocystis* mutant strains lacking either Flv1 or Flv3 (Δ*flv1* and Δ*flv3*, respectively, Helman et al., 2003) or NDH-1L and NDH-1L´ (Δ*d1d2*, lacking NdhD1 and NdhD2, Ohkawa et al., 2000), as well as triple mutant strains with combined deficiencies of both pathways (Δ*flv1 d1d2* and Δ*flv3 d1d2*). Our results provide convincing evidence that the presence of either Flv1/3 orNDH-1L is indispensable for survival of *Synechocystis* cells under transitions from abundant [CO_2] conditions to combined stress conditions of high irradiance and lowered [CO_2]. We show that dynamically coordinated cooperative function of NDH-1L and Flv1/3 is required for photoprotection of the photosynthetic apparatus of *Synechocystis* cells during transitions to LC and high light conditions.

RESULTS

Simultaneous inactivation of Flv1/3 and NDH-1L is lethal upon shift from high to air [CO_2] and high irradiance

In order to examine whether simultaneous inactivation of NDH-1 and FDPs has an adverse effect on cell survival, we monitored the growth of *Synechocystis* wild-type (WT) and the mutants lacking functional Flv1/3 and/or NdhD1/D2 in conditions of differing CO_2 availability and light intensity.

The triple mutants Δ*flv1 d1d2* and Δ*flv3 d1d2* exhibited slightly slower growth compared to the other strains under elevated [CO_2] (3% CO_2 and 50 µmol photons $m^{-2}s^{-1}$ PAR) (Figure 1A). We detected no differences in growth when the 3% CO_2-pre-grown cells were diluted (OD_{750}=0.1) and shifted to air [CO_2] conditions with the same light intensity (Figure 1B). In contrast, when cultures pre-grown in 3% [CO_2] were diluted (OD_{750}=0.1) and subjected to air [CO_2] and high light (HL, intensity of 220 µmol photons $m^{-2}s^{-1}$) simultaneously, we detected a strong growth phenotype in both triple mutants. Growth of Δ*flv3 d1d2* and Δ*flv1 d1d2* was completely inhibited (Figure 1D). Importantly, Δ*flv1*, Δ*flv3* and Δ*d1d2* strains demonstrated similar to WT growth under air [CO_2] /HL conditions. It was next examined whether pre-adaptation to air [CO_2] would rescue the growth arrest. When cells previously adapted to air [CO_2] and moderate light (50 µmol photons $m^{-2}s^{-1}$) were diluted (OD_{750}=0.1) and shifted to air [CO_2] /HL, no differences in growth patterns between the strains were detected (Figure 1C).

Importantly, mutants lacking Flv1/3 and NDH-1MS (Δ*flv1 d3d4* and Δ*flv3 d3d4* strains) (Figure S1A-B) did not show any substantial growth phenotype compared to WT after a shift from 3% [CO_2] to air [CO_2]/HL, suggesting that crosstalk between FDPs and NDH-1MS is not as important as with NDH-1L. Our attempts to create a M55/Δ*flv1* and M55/Δ*flv3* double mutants lacking Flv1 or Flv3 and both NDH-1L and NDH-1MS were not successful. We could not obtain any M55/Δ*flv1* colonies and the M55/Δ*flv3* mutant strain could not be segregated and demonstrated poor growth, suggesting that the absence of both pathways, NDH-1 and FDPs, disturbs essential cell metabolism (Figure S1C).

We also studied the growth of the mutants on agar plates containing BG-11 (Figure 1E). For these experiments 3% CO_2-grown cells were diluted and grown on plates either under air [CO_2]/ moderate light or air [CO_2]/HL conditions for 7 days. The Δ*flv1* and Δ*flv3* mutants did not exhibit any visible differences in growth capacity under these conditions in comparison to WT. In contrast, growth of the triple mutants was reduced under air [CO_2] / 50 µmol photons $m^{-2}s^{-1}$ while no growth was detected under air [CO_2] / 220 µmol photons $m^{-2}s^{-1}$ (Figure 1E). As the growth phenotypes of Δ*flv1* and Δ*flv3* as well as those of Δ*flv1 d1d2* and Δ*flv3 d1d2* were similar in all conditions, we only included Δ*flv3* and Δ*flv3 d1d2* in most of the subsequent experiments.

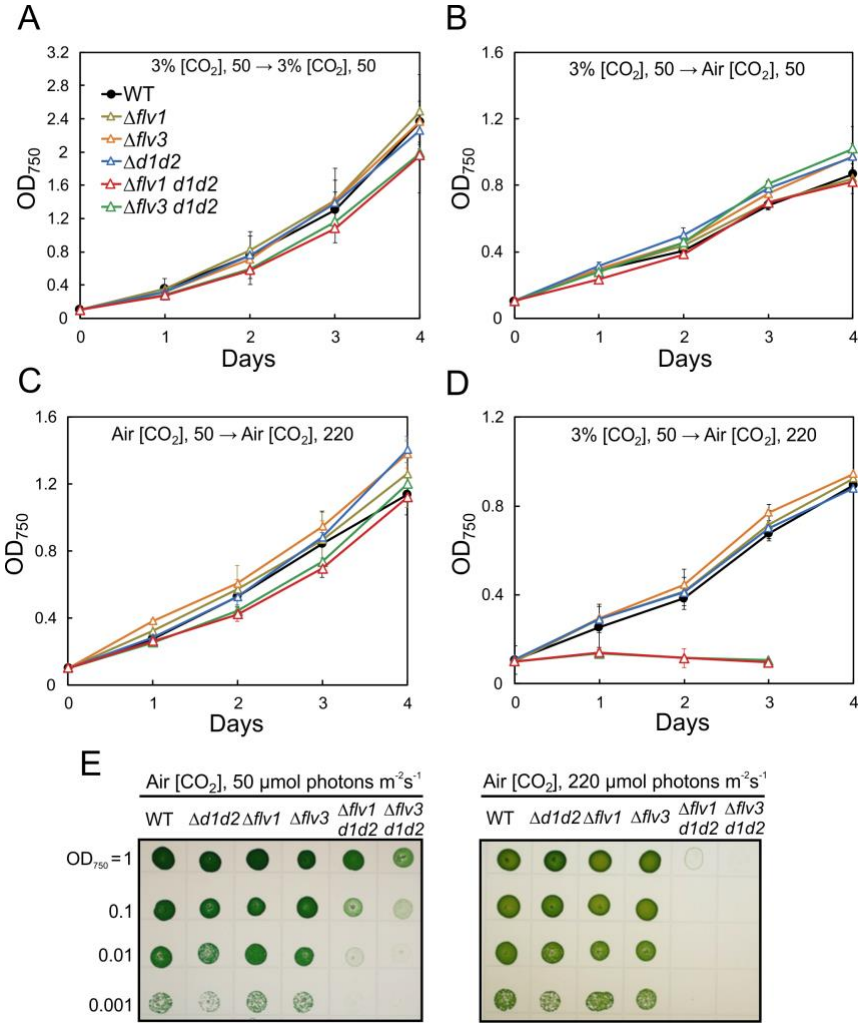

Figure 1. Growth of WT and mutant strains in different experimental conditions. All experimental cultures were started from pre-cultures in BG-11 pH 7.5 adjusted to OD_{750}=0.1. **(A)** Cells were pre-cultivated under 3% [CO_2] and 50 µmol photons $m^{-2}s^{-1}$, adjusted to OD_{750}=0.1 and grown in the same conditions. **(B)** Cells were pre-cultivated under 3% [CO_2] and 50 µmol photons $m^{-2}s^{-1}$ and shifted to air [CO_2] and 50 µmol photons $m^{-2}s^{-1}$. **(C)** Cells were pre-cultivated under air [CO_2] and 50 µmol photons $m^{-2}s^{-1}$ and shifted to air [CO_2] and 220 µmol photons $m^{-2}s^{-1}$. **(D)** Cells were pre-cultivated under 3% [CO_2] and 50 µmol photons $m^{-2}s^{-1}$ and shifted to air [CO_2] and 220 µmol photons $m^{-2}s^{-1}$. The values presented in A–D are means of three independent biological replicates ±SE. **(E)** Growth of WT and mutant cells on BG-11 (pH 7.5) agar plates. Cells grown under 3% [CO_2] / 50 µmol photons $m^{-2}s^{-1}$ were harvested and spotted on BG-11 agar plates in series of ten-fold dilutions from cells at OD_{750}=1, and incubated under air [CO_2] and 50 µmol photons $m^{-2}s^{-1}$ and air [CO_2] and 220 µmol photons $m^{-2}s^{-1}$ for 7 days. See also Figure S1.

Flv1/3 or NDH-1L is required for oxidation of PSI during sudden increases in light intensity

The lethal phenotype upon shift to air [CO_2] / HL caused by simultaneous impairment of the Mehler-like reaction catalyzed by Flv1/3 hetero-oligomers (Helman et al., 2003; Allahverdiyeva et al., 2013; Allahverdiyeva et al., 2015) and respiration and CET mediated by the NDH-1L complex (Ohkawa et al., 2000) suggested existence of functional redundancy between these electron transfer pathways. To further investigate this possibility, we used membrane inlet mass spectrometry (MIMS) to examine the kinetics of O_2 and CO_2 exchange upon HL-illumination of dark-adapted WT and mutant cells grown for four days in air [CO_2] / 50 µmol photons $m^{-2}s^{-1}$. In order to distinguish O_2 uptake from gross O_2 evolution under illumination, we enriched the cell suspensions with $^{18}O_2$ prior to the measurements. In dark-adapted WT cells, a transient peak in O_2 uptake occurs during the first minute of illumination (Figure 2A). We showed recently that the transient peak is attributable to the Mehler-like reaction catalyzed predominantly by Flv1/3 hetero-oligomers, while Flv2/4 hetero-oligomers mainly contribute to steady-state rate of light-induced O_2 reduction in a interdependent manner (Santana-Sanchez et al., 2019). In Δ*flv3* cells, light-induced O_2 reduction was almost abolished, and slight impairment of the rate of photosynthetic gross O_2 evolution was observed in comparison to WT cells (Figure 2B), in agreement with previous studies (Helman et al., 2003; Allahverdiyeva et al., 2013; Santana-Sanchez et al., 2019).

In Δ*d1d2* cells, light-induced O_2 uptake sustained at a substantially high level (c.a. 75–100 µmol O_2 mg Chl^{-1} hr^{-1}) throughout the illumination period, while gross O_2 evolution was diminished nearly two-fold compared to WT (Figure 2C). The elevation of O_2 uptake in Δ*d1d2* was most likely due to increased activity of FDPs. Indeed, Δ*flv3 d1d2* mutant cells showed only minor light-induced O_2 uptake transiently during the first minute of illumination (Figure 2D). Δ*flv3 d1d2* cells demonstrated slower induction of photosynthetic O_2 evolution following two-component kinetics, and slightly impaired steady-state gross O_2 evolution compared to WT (Figure 2D). In order to dissect the contribution of Flv2/4 to O_2 uptake in the FDP/NDH-1 mutant strains, we monitored O_2 exchange also in a Δ*flv2 d1d2* triple mutant. In these cells the initial strong O_2 uptake at the dark-light transition, which is mainly mediated by Flv1/3, occurred similarly to WT and Δ*d1d2* cells, but steady-state O_2 uptake, which is catalyzed by Flv2/4 (Santana-Sanchez et al., 2019), was diminished (Figure S2A).

The initial peak in CO_2 uptake rate at the onset of illumination likely reflects activation of the CCM (Liran et al., 2018). Accordingly, the CCM-deficient Δ*d3d4* mutant is lacking this initial peak (data not shown). No salient impairment of CCM was observed in any of the strains, with CO_2 uptake

rates peaking at c.a. 1.5 mM CO_2 mg Chl^{-1} hr^{-1}. In WT as well as in Δ*flv3*, CO_2 fixation is then induced and the respiratory compensation point surpassed after ~1 min of illumination (Figure 2A–B). In Δ*d1d2*, however, induction of CO_2 fixation is severely delayed, and the cells only reached the compensation point at the end of the 5 min illumination period (Figure 2C). Intriguingly, although a slight delay was observed also in Δ*flv3 d1d2* as well as Δ*flv2 d1d2*, induction of CO_2 fixation was largely recovered in the triple mutants (Figure 2D and Figure S2A).

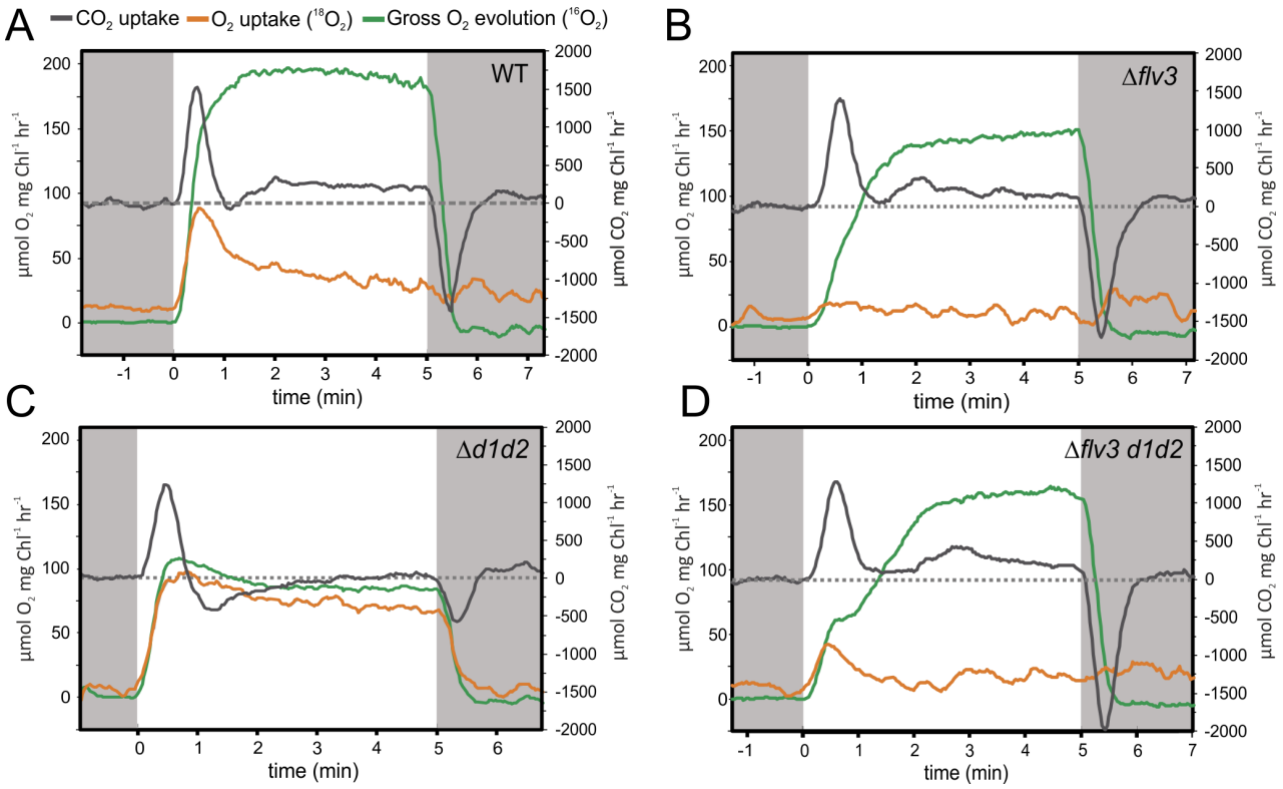

Figure 2. O_2 and CO_2 exchange rates in WT and mutant strains. Cells were grown in air [CO_2] / 50 µmol photons m^{-2}s^{-1} for 4 days in BG-11 pH 7.5, after which the cells were harvested and Chl *a* concentration adjusted to 10 µg ml^{-1} with fresh BG-11. Cells were dark-adapted for 15 min, and gas exchange was monitored by membrane inlet mass spectrometry (MIMS) over a 5 min illumination period with 500 µmol photons m^{-2}s^{-1} of white actinic light. . Prior to the measurements, samples were supplemented with $^{18}O_2$ at an equivalent concentration to $^{16}O_2$ to distinguish O_2 uptake from O_2 evolution, and with 1.5 mM $NaHCO_3$. The dashed line in each panel indicates the compensation point of CO_2 fixation (uptake rate equals respiratory rate). The experiment was repeated with three independent biological replicates, of which representative measurements are shown. See also Figure S2.

These results from MIMS indicated that combined deficiency of Flv1/3 and NDH-1L grown under air [CO_2] / 50 µmol photons m^{-2}s^{-1} only slightly perturbs photosynthetic electron transfer and the redox poise between the PETC and cytosolic sink reactions. We therefore proceeded to further

examine the ability of the mutant strains to adjust their photosynthetic activity to variable light conditions by measuring chlorophyll *a* (Chl) fluorescence simultaneously with P700 redox changes in conditions where light intensity periodically fluctuated between low (25 µmol photons $m^{-2}s^{-1}$, LL) and high irradiance (530 µmol photons $m^{-2}s^{-1}$, HL). Cells lacking Flv3 suffered from transient PSI acceptor side limitation Y(NA) upon sudden increases in light intensity, resulting in delayed oxidation of PSI (Figure 3A), which is in line with previous studies (Helman et al. 2003, Allahverdiyeva et al. 2013). During subsequent 1 min cycles of LL/HL, however, the ability of Δ*flv3* to oxidize PSI in HL improved, suggesting that cells were able to acclimate to the fluctuating light condition via a compensatory mechanism that is distinct from Flv1/3 hetero-oligomers, such as *e.g*. electron transfer through NDH-1 .

We detected no acceptor-side limitation during the HL phases in Δ*d1d2* (Figure 3A), or in Δ*flv2 d1d2* cells (Figure S2B), as PSI was oxidized similarly to WT (Figure 3B). Interestingly, however, Δ*d1d2* cells exhibited slightly elevated acceptor-side limitation during the LL phases of the experiment (Figure 3A), supporting a role for NDH-1L in maintaining photosynthetic redox poise in light-limited conditions. In the triple mutant strain Δ*flv3 d1d2*, transitions from low to high irradiance as well as from dark to light caused severe limitation on the acceptor side of PSI, resulting in an inability to oxidize PSI during 1 min in HL, or to acclimate to the fluctuating light during subsequent cycles. Interestingly, diminished donor side limitation in Δ*flv3 d1d2* resulted in slightly elevated effective yield of PSI during the HL phases (Figure 3C). This could indicate attenuation of pH-dependent limitation of electron transfer at Cyt b_6f, due to impairment of proton motive force (*pmf*) generation in CET and the Mehler-like reaction. Effective yield of PSII was slightly decreased in HL in Δ*flv3 and* Δ*d1d2*, but not in Δ*flv3 d1d2* (Figure 3D).

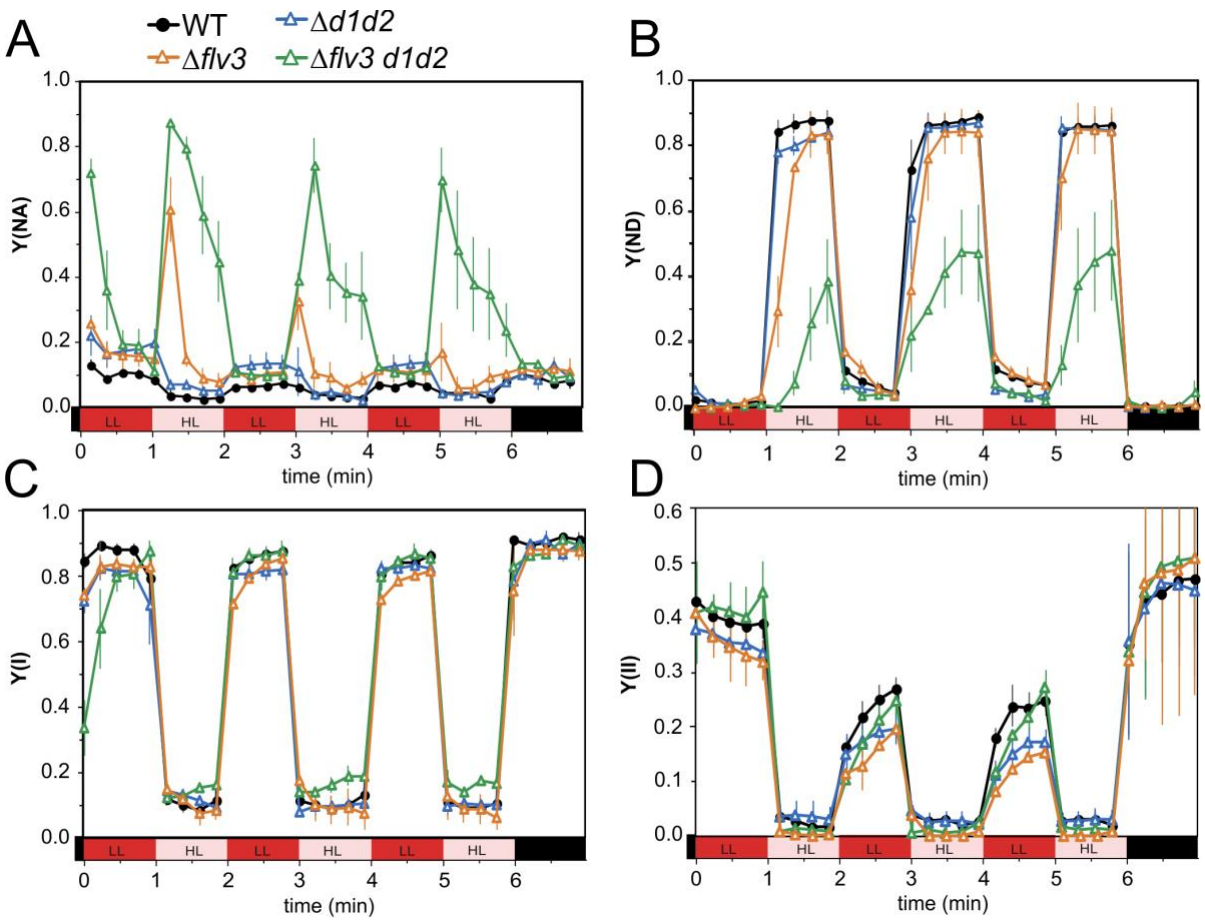

Figure 3. Photosynthetic parameters in WT and mutants strains in fluctuating light. (A) Acceptor side limitation of PSI, Y(NA), **(B)** donor side limitation of PSI, Y(ND), as well as **(C)** quantum yield of PSI, Y(I) were calculated from absorbance difference changes at 875-830 nm according to (Klughammer and Schreiber, 2008). Chl *a* fluorescence changes were measured simultaneously with PSI redox changes and used to calculate **(D)** quantum yield of PSII. Cells were grown in air [CO_2] / 50 µmol photons $m^{-2}s^{-1}$ for 4 days in BG-11 pH 7.5, after which the cells were harvested and Chl *a* concentration adjusted to 10 µg ml^{-1} with fresh BG-11. Cells were dark-adapted for 10 min, and then subjected to illumination with red actinic light whose intensity was alternating between 25 and 530 µmol photons $m^{-2}s^{-1}$ in 1 min periods. Saturating pulses (500 ms of 5000 µmol photons $m^{-2}s^{-1}$) were provided every 15 seconds. The values shown are averages from 3–4 independent biological replicates ±SE. See also Figure S2.

The differences in photosynthetic electron transfer reported above may also be contingent on altered redox state of the $NADP^+$/ NADPH pool in different FDP and NDH-1 mutants. Therefore, in order to investigate the effect of Flv1/3 and/or NDH-1L deficiency on $NADP^+$/NADPH redox kinetics, we recorded NADPH fluorescence changes from dark-adapted cells simultaneously with Chl *a* fluorescence in conditions where actinic light intensity fluctuated between 25 (LL) and 530 µmol photons $m^{-2}s^{-1}$ (HL) similarly to Figure 3. Upon dark-to-LL transitions, NADPH rapidly

accumulated close to a maximal amount in all strains. Re-oxidation of NADPH then occurred in WT and Δ*flv3d1d2* cells after c.a. 2 s of illumination, while in Δ*flv3* a slower oxidation phase preceded a transient re-reduction phase during the first minute of illumination (Figure 4A–B). Strong reduction of the $NADP^+$ pool was also detected in Δ*flv3* during the second HL phase of the experiment. In Δ*d1d2* cells, very little oxidation of the NADPH pool occurred during illumination, even at HL-LL transitions (Figure 4C). Chl *a* fluorescence also remained at an elevated level (Figure 4C), suggesting a reduced PQ pool. This was possibly due to delayed activation of CO_2 fixation in the Calvin-Benson cycle (Figure 2C), and impaired CET or dark respiration. In contrast, NADPH was strongly oxidized in Δ*flv3 d1d2* cells at HL-LL transitions (Figure 4D), but was predominantly reduced in dark-adapted cells (Figure 4D). Upon cessation of illumination, oxidation of the NADPH pool was followed by transient re-reduction after c.a. 10 s. As observed previously (Schreiber and Klughammer, 2009), the re-reduction peak coincided with a secondary post-illumination rise in Chl a fluorescence (PIFR), while oxidation of NADPH paralleled an initial PIFR. The post-illumination re-reduction of NADPH was diminished and both Chl *a* PIFR peaks were missing in Δ*d1d2* (Figure 4C). Therefore, the initial PIFR likely originates from respiratory electron transfer via NDH-1L. Both Chl PIFR peaks were however observed in Δ*flv3 d1d2* cells, indicating involvement of a complementary pathway, possibly via succinate dehydrogenase (Cooley and Vermaas, 2001), or a CEF pathway dependent on PGR5 and PGRL1-LIKE (Yeremenko et al., 2005; Dann and Leister, 2019). Finally, we monitored NADPH redox kinetics under conditions mimicking the MIMS experiments, where strong O_2 photoreduction occurs in WT and Δ*d1d2* during the first minute of dark-to-HL transition (Figure 2). No substantial differences were observed between the strains, as close to maximal reduction of $NADP^+$ was obtained within ~0.25 s (Figure 4F) and maintained throughout a 40 s illumination period (Figure 4E). This argues against NADPH being a primary electron donor to either Flv1/3 or NDH-1L.

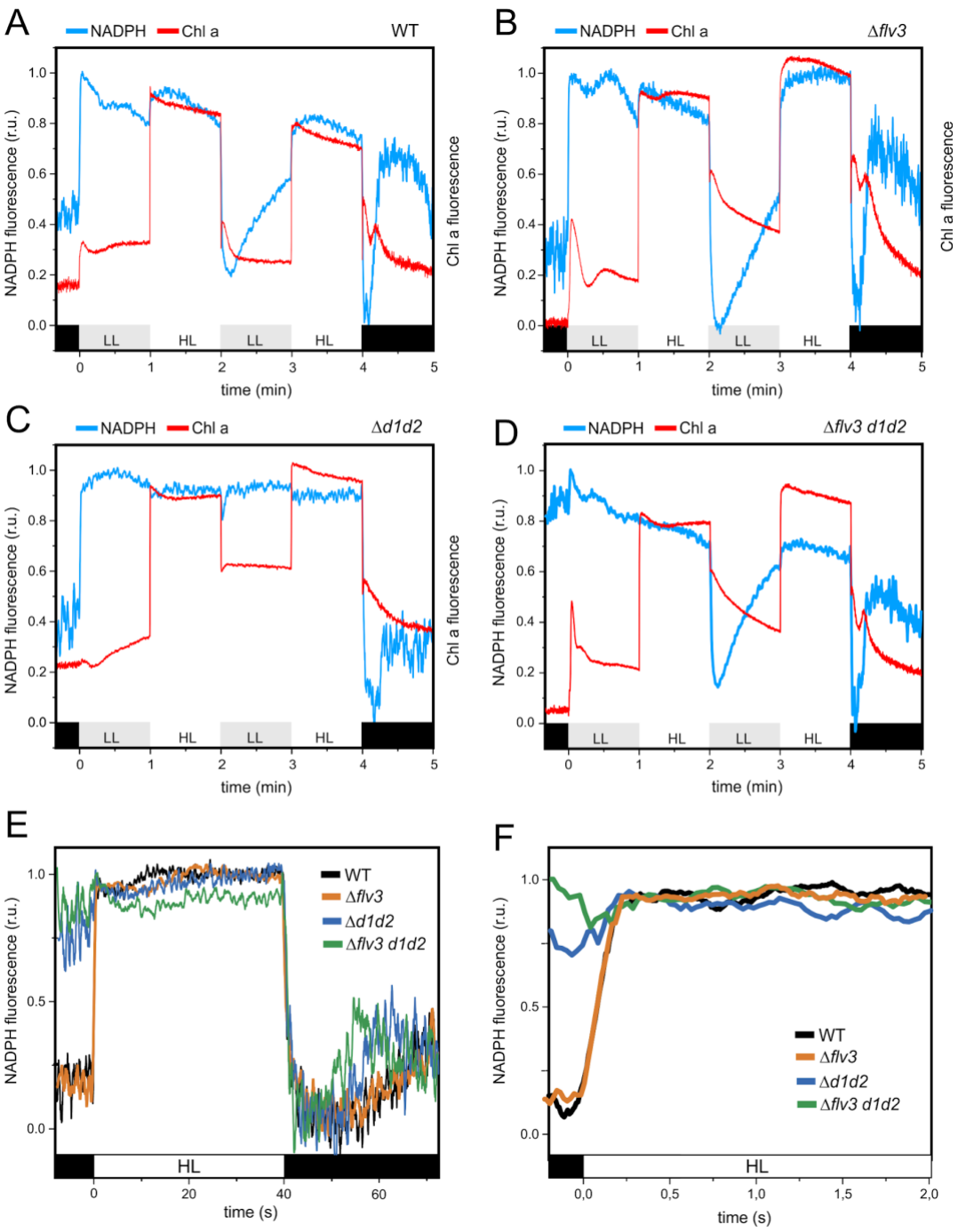

Figure 4. NADPH and Chl *a* fluorescence under fluctuating light in WT and mutant strains. WT **(A)**, Δ*flv3* **(B)**, Δ*d1d2* **(C)**, and Δ*flv3 d1d2* cells **(D)** were grown in air [CO_2] / 50 µmol photons $m^{-2}s^{-1}$ for 4 days in BG-11 pH 7.5, after which the cells were harvested and Chl a concentration adjusted to 5 µg ml^{-1} with fresh BG-11. Cells were dark-adapted for 10 min, and then subjected to illumination with red actinic light alternating between 25 and 530 µmol photons $m^{-2}s^{-1}$ in 1 min periods. NADPH redox changes were monitored with the Dual-PAM 100 spectrometer and its 9-AA/NADPH accessory module by measuring fluorescence changes between 420 and 580 nm induced by excitation at 365 nm, as described by (Schreiber and Klughammer, 2009) and (Kauny and Setif, 2014). Chl *a* fluorescence was recorded simultaneously. **(E)**

NADPH redox changes during illumination of dark-adapted cells with 530 µmol photons $m^{-2}s^{-1}$. Other experimental details are as in A-D. **(F)** shows a magnification of the first 2 s of illumination in (E). The values are normalized according to minimum and maximum fluorescence changes at the onset and cessation of illumination, respectively. The experiments were repeated with three independent biological replicates, of which representative measurements are shown. r.u. = relative units.

Redox status of PSI donor and acceptor side electron carriers and buildup of *pmf* during dark-to-light transitions depend on both Flv1/3 and NDH-1

To elucidate the molecular mechanism behind the photosynthetic phenotypes of the mutant strains, we next utilized a DUAL-Klas-NIR 100 spectrophotometer to distinguish between redox changes of plastocyanin (PC), P700, and ferredoxin (Fd) (Klughammer and Schreiber, 2016; Schreiber, 2017; Setif et al., 2019) upon exposure of dark-adapted cells to high irradiance (503 µmol photons $m^{-2}s^{-1}$). Upon illumination of WT cells, rapid oxidation of P700 and PC occurred, followed by transient reduction of PC, P700, as well as Fd after ~0.2 s (Figure 5A). Re-oxidation of all three electron carriers then ensued after ~0.5 s. In Δ*flv3* cells P700 and PC remained mostly reduced after the initial oxidation transient until ~3 s, when another transient and partial re-oxidation peak of P700 and PC occurred at ~8 s (Figure 5B). This was followed by re-reduction of P700, similarly to that observed recently by Bulychev et al. (2018). After 15 s in light, P700 and PC became gradually oxidized. In contrast to WT, Fd remained reduced for several seconds in light, and was only slowly re-oxidized over the 30 s illumination period (Figure 5B). These observations indicate the importance of Flv1/3 as an electron sink to O_2, accepting electrons presumably from reduced Fd (after ~0.5 s in light). In Δ*d1d2*, redox changes of PC, P700 and Fd were similar to WT, except that the reduction of $P700^+$ following initial oxidation as well as reduction of Fd occurred already after ~50 ms (Figure 5C). In Δ*flv3 d1d2*, re-reduction of $P700^+$ and reduction of Fd also occurred already after ~50 ms (Figure 5D), suggesting involvement of NDH-1L as an acceptor of electrons from Fd at that stage. Fd was reduced more quickly in Δ*flv3 d1d2* than in any of the other strains and was slowly re-oxidized over 30 s (Figure 5D), likely due to limitation on the acceptor side of PSI (Figure 3A). In summary, these NIR-spectroscopic measurements revealed that Flv1/3 and NDH-1L control the redox poise between PSI, PC, and primary electron acceptor Fd during specific timeframes at transitions to high irradiance. The results are congruent with Fd functioning as the electron donor to both NDH-1L and Flv1/3.

To inspect whether the phenotypes observed above depend on differential buildup or regulation of *pmf*, we measured *in vivo* changes in the *pmf* by monitoring the absorbance change difference between 500-480 nm, which constitutes the electrochromic shift (ECS) in *Synechocystis* (Viola et al., 2019). *In vivo* measurement of light-induced ECS revealed that after 1 s of illumination of dark-adapted WT cells with 500 µmol photons $m^{-2}s^{-1}$, high *pmf* level was transiently generated, followed by decline during subsequent seconds (Figure 5E). After ~10 s of illumination *pmf* again increased towards a steadier value (Figure 5E). Congruently with the strong reduction of P700 and Fd (Figure 5B), the initial *pmf* peak after the first second of illumination was heavily dependent on the presence of Flv1/3. In both Δ*flv3* and Δ*flv3 d1d2 pmf* and thylakoid proton flux (vH+) were lower than in WT after 1 s (Figure 5G). In Δ*flv3 pmf* remained lower than WT for the first 20 s of illumination, but did not differ from WT between 30–60 s due to diminished conductivity of the thylakoid membrane (gH+) (Figure 5F), which is mainly determined by the activity of the ATP synthase (Cruz et al., 2005; Viola et al., 2019). In Δ*d1d2* thylakoid proton flux was similar to WT (Figure 5G), likely due to enhanced FDP activity (Figure 2C) compensating for impaired CET and respiration. However, *pmf* remained lower than in WT throughout the 1 min experiment (Figure 5E) because of elevated conductivity (Figure 5F). In contrast, despite drastically lower proton flux (Figure 5G), Δ*flv3 d1d2* cells maintained *pmf* close to WT level after the first seconds in light (Figure 5E) due to diminished conductivity (Figure 5F). This indicates that the increased acceptor side limitation of PSI in Δ*flv3 d1d2* in comparison to Δ*flv3* (Figure 3A) is not caused by lack of photosynthetic control as a consequence of lowered *pmf* generation in CET. Based on comparison of ECS kinetics in single, double, and triple mutant cells studied here, we conclude that both Flv1/3 and NDH-1L contribute to proton flux during transitions to high irradiance. However, lack of NDH-1L in Δ*d1d2* is mostly compensated by elevated FDP-activity in terms of proton flux. In contrast, impaired thylakoid proton flux in Δ*flv3* during dark-to-light transitions cannot be compensated by NDH-1. Instead, downregulation of ATP-synthase activity lowers thylakoid conductivity and allows maintenance of *pmf* (apart from the first seconds of illumination) in Δ*flv3* and, even more dramatically, in Δ*flv3 d1d2*.

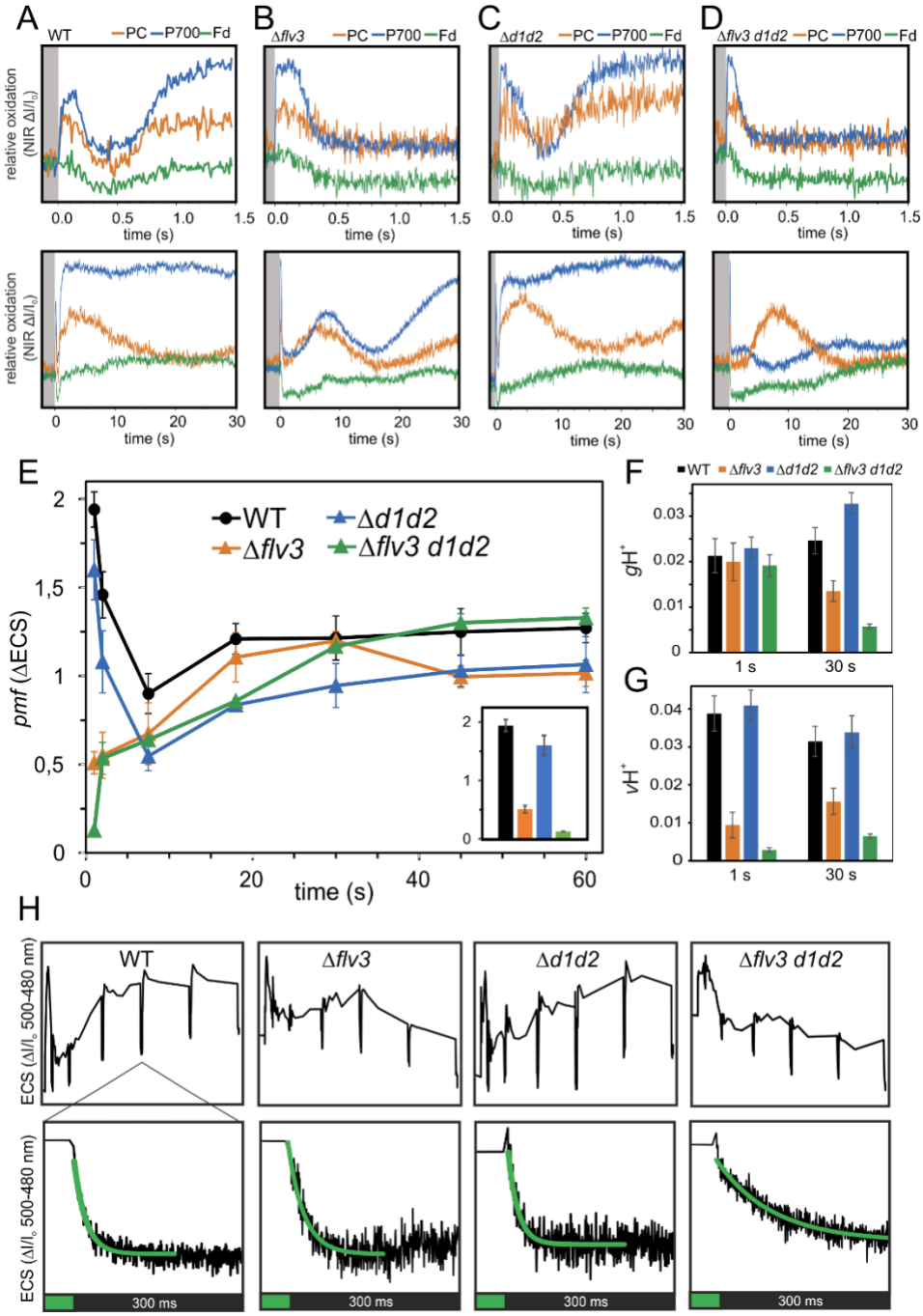

Figure 5. Redox changes of PC, P700, and Fd, and buildup of *pmf* during dark-to-HL transitions. WT **(A)**, Δ*flv3* **(B)**, Δ*d1d2* **(C)**, and Δ*flv3 d1d2* cells **(D)** were dark-adapted for 10 min, after which absorbance difference changes at 780–800 nm, 820–870 nm, 840–965 nm and 870–965 nm were measured with the Klas-NIR 100 spectrometer during 30 s illumination at 503 µmol photons $m^{-2}s^{-1}$ of red actinic light. The PC, P700, and Fd signals were deconvoluted from the absorbance difference changes using differential model plots (DMPs) determined for this study (Figure S3). The upper panels in A–D show magnifications of the first 1.5 seconds of illumination from the lower panels. The experiment was repeated with three independent biological replicates, of which representative traces are shown. See also Figure S3. **(E)** Buildup of *pmf* during transitions from dark to 500 µmol photons $m^{-2}s^{-1}$ of green actinic light. Absorbance difference

between 500-480 nm (ECS) was measured with a JTS-10 spectrometer, and light-induced *pmf* was determined from the dark interval relaxation kinetics (DIRK) of the ECS signal. Means ±SEM from 3–4 independent experiments are shown. The small inset shows *pmf* values after 1s of illumination for a clearer view. **(F)** Conductivity of the thylakoid membrane (gH+) after one and 30 s of illumination as in (E). gH+ was determined as the inverse of the time constant of first-order post-illumination decay kinetics of the ECS signal. **(G)** Thylakoid proton flux (vH+), calculated as *pmf* vx gH+. **(H)** Representative traces of 500-480 nm absorbance differences used to determine the values in (E) and post-illumination ECS decay kinetics during a 500 ms dark interval after 30 s in light (lower panels). First-order fits are shown in green. Cells were grown in air [CO_2] / 50 µmol photons $m^{-2}s^{-1}$ for 4 days in BG-11 pH 7.5, after which cells were harvested and Chl *a* concentration adjusted to 10 µg ml^{-1} with fresh BG-11 for A–D and to 7.5 µg ml^{-1} for E–J.

PSI content is diminished in Δ*flv1/3 d1d2* cells shifted to high irradiance and air [CO_2]

The results from the growth assays, along with the real-time gas exchange and P700 redox change measurements suggested that in Δ*d1d2* cells, an increase in the activity of FDPs compensate for the absence of a functional NDH-1L complex, allowing efficient oxidation of PSI under high irradiance. Conversely, in Δ*flv1* and Δ*flv3* mutants, over-reduction of the electron transfer chain occurs initially upon exposure to high irradiance, but another mechanism eventually allows acclimation and survival in high light and high [CO_2] (Helman et al., 2003). Under air [CO_2] Flv1/Flv3 hetero-oligomers catalyse transient O_2 photoreduction. Therefore no strong growth phenotype is observed in Δ*flv1* or Δ*flv3* under constant high irradiance (Allahverdiyeva et al. 2013, Sanchez et al. 2019). However, when both NDH-1L and Flv1/3 are absent and the electron sink capacity of the cytosol is not elevated by high [CO_2], cells are unable to oxidize PSI in high light, possibly resulting in lethal photodamage to PSI. To assess this hypothesis, we employed immunoblotting to provide estimates of the protein content of PSII (D1) and PSI (PsaB) subunits, orange carotenoid protein (OCP), large isoform of the ferredoxin-NADP+ oxidoreductase (FNR_L), FDPs, as well as NdhD3 and the bicarbonate transporter SbtA after 24 hours exposure to different growth conditions.

WT and Δ*flv1* or Δ*flv3* cells grown at 3% [CO_2] / 50 µmol photons $m^{-2}s^{-1}$ and shifted to standard growth conditions (air [CO_2] / 50 µmol photons $m^{-2}s^{-1}$) at OD=0.1, demonstrated similar accumulation level of the PSII reaction center protein D1 or the PSI subunit PsaB. In contrast, we detected a moderate decrease in the amount of both D1 and PsaB already in standard conditions in the Δ*flv1 d1d2* and Δ*flv3 d1d2* triple mutants, while an increased amount of both proteins was

detected in Δ*d1d2* (Figure 6A). After 24 hours exposure to air [CO_2] / HL (220 µmol photons $m^{-2}s^{-1}$), PsaB amount had decreased even further in Δ*flv1 d1d2* and Δ*flv3 d1d2* (Figure 6C). Furthermore, 77K fluorescence spectra revealed that while Δ*flv3 d1d2* and WT cells grown under air [CO_2] / 50 µmol photons $m^{-2}s^{-1}$ had similar PSI/PSII ratios (Figure 6D), the 24-hour exposure to air [CO_2] / HL caused a dramatic decrease in the relative PSI fluorescence cross section (Figure 6E). This strongly supports the hypothesis that lethality in these conditions is caused by damage to PSI. Interestingly, a substantial decrease in D1 content in air [CO_2] / HL was also observed in the triple mutants (Figure 6B–C), suggesting downregulation of PSII possibly in an attempt to limit excessive supply of electrons to PSI (Tikkanen et al., 2014).

Importantly, the Δ*flv1 d1d2* and Δ*flv3 d1d2* strains were unable to induce substantial accumulation of the proteins encoded by the *flv4-2* operon after 24 hours in air [CO_2] (Figure 6A and 6C). Only when pre-grown for 4 days in air [CO_2] / 50 µmol photons $m^{-2}s^{-1}$ before being shifted to higher irradiance, the expression of the operon was induced (Figure 6B). Similarly to *flv4-2* operon proteins, both NdhD3 and SbtA failed to accumulate after shifts from 3% to air [CO_2] / HL in the triple mutants, which likely impairs CCM and contributes to the lethal phenotype of the triple mutants in those conditions. Small amounts of NdhD3 and SbtA were detected in triple mutant cells shifted from 3% [CO_2] to air [CO_2] / 50 µmol photons $m^{-2}s^{-1}$ (Figure 6A). Close to WT amount of NdhD3 but only a small amount of SbtA was detected after 4+1 days in air [CO_2] / 220 µmol photons $m^{-2}s^{-1}$ (Figure 6B). Interestingly, this was still sufficient for almost fully functional CCM, deduced from CO_2 uptake kinetics in the conditions of the MIMS experiments (Figure 2D). In the Δ*d1d2* mutant NdhD3 content was similar to WT, but Flv3 as well as the *flv4-2* operon proteins (Flv2, Flv4, and Sll0218) were upregulated in all conditions tested (Figure 6A–C), which likely contributes to the increased rate of O_2 photoreduction in that strain (Figure 2C). The amounts of OCP and of FNR_L were unchanged in the mutant strains in all conditions (Figure 6).

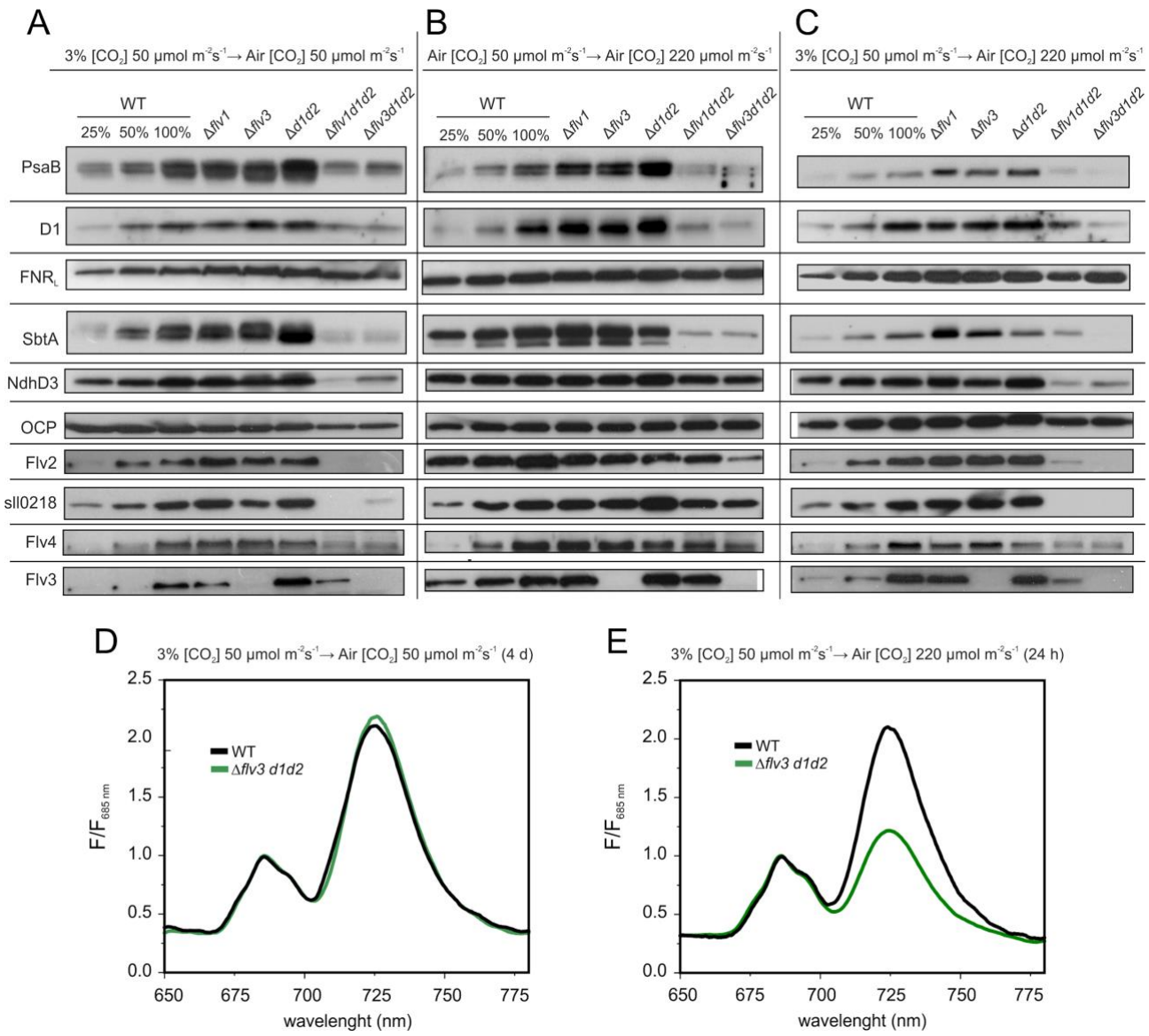

Figure 6. Immunodetection of proteins related to photosynthesis and CCM and 77K fluorescence emission spectra in WT and mutant strains. Pre-cultures were first grown for 3 days in BG-11 pH 7.5 at 3% [CO_2] / 50 µmol photons $m^{-2}s^{-1}$ and then pelleted, resuspended in fresh BG-11 pH 7.5 at OD_{750}=0.15 and **(A)** incubated for 24 hours in air [CO_2] / 50 µmol photons $m^{-2}s^{-1}$, **(B)** grown for 4 days in air [CO_2] / 50 µmol photons $m^{-2}s^{-1}$, harvested, resuspended in BG-11 at OD_{750}=0.15 and then incubated for 24 hours in air [CO_2] / 220 µmol photons $m^{-2}s^{-1}$, **(C)** incubated for 24 hours in air [CO_2] / 220 µmol photons $m^{-2}s^{-1}$. Total protein extracts were separated by SDS-PAGE and probed with specific antibodies. The immunoblots shown are representative of 2–3 independent biological replicates. **(D)** 77K fluorescence emission spectra from intact WT and Δ*flv3 d1d2* cells grown for 4 days in air [CO_2] / 50 µmol photons $m^{-2}s^{-1}$. **(E)** After pre-growth at 3% [CO_2] / 50 µmol photons $m^{-2}s^{-1}$ cells were pelleted, resuspended in fresh BG-11 pH 7.5 at OD_{750}=0.15 and incubated for 24 hours in air [CO_2] / 220 µmol photons $m^{-2}s^{-1}$. The cells (D and E) were pelleted, adjusted to [Chl *a*] of 7.5 µg ml^{-1}, and excited with 440 nm light at 77K. The spectra were normalized to the PSII fluorescence peak at 685 nm.

DISCUSSION

Flv1/3 hetero-oligomers have been shown to be essential for photoreduction of O_2 as a rapid response to excessive reduction of PSI, and consequently, for cell survival under fluctuating light conditions (Allahverdiyeva et al., 2013; Santana-Sanchez et al., 2019). Moreover, we recently showed that in low [CO_2], Flv2/4 hetero-oligomers also catalyze light-induced steady-state reduction of O_2 on the acceptor side of PSI in a coordinated manner with Flv1/3 (Santana-Sanchez et al., 2019). In turn, the NDH-1L complex incorporates either the NdhD1 or NdhD2 subunit and functions in respiratory electron transfer (as complex I), as well as in cyclic electron flow around PSI, using Fd as electron donor (Ohkawa et al., 2000; Ma and Ogawa, 2015; He et al., 2015; Peltier et al., 2016; Laughlin et al., 2019; Saura and Kaila, 2019; Schuller et al., 2019). In the current study, we have used *Synechocystis* mutant strains with combined deficiency of Flv1/3 hetero-oligomers and NDH-1L to examine the physiological significance of the two electron transfer pathways and the possibility of functional interdependence between them. Our results provide compelling evidence that Flv1/3 and NDH-1L have concomitant physiological functions coordinated in a dynamic manner that allows efficient oxidation of PSI (and thus protection of it from photodamage) under variable light conditions, and when low [CO_2] limits the consumption of reductants in the CBC. The two pathways can compensate for each other's absence to some extent, but absence of both Flv1/3 hetero-oligomer and NdhD1/NdhD2 is lethal when cells are transferred from elevated [CO_2] to conditions of air level [CO_2] and high irradiance (Fig1D-E). Besides the absence of these two important pathways, lethality is due to an inability to accumulate low C_i-inducible photoprotective CCM proteins (Fig. 6C).

Coordinated functions of Flv1/3 and NDH-1L protect PSI by maintaining redox poise between the PETC and carbon fixation

Cells lacking functional Flv1/3 hetero-oligomers suffer from transient over-reduction of PSI during sudden increases in light intensity (Figure 3 and Figure 5) due to impairment of the Mehler-like reaction (Figure 2) (Allahverdiyeva et al., 2013). It has been suggested that NAD(P)H is the electron donor to Flv3 (Vicente et al., 2002; Brown et al., 2019) and Flv1 (Brown et al., 2019). However, Fd was not investigated as a possible electron donor in these *in vitro* assays. *In vivo* experiments performed in this study demonstrate that a quick re-oxidation of Fd after 0.5 s (Figure 5A) in light is absent in the Δ*flv3* deletion strains, instead Fd stays strongly reduced (Figure 5B). As

no impairment of NADPH reduction and oxidation kinetics in similar conditions was detected in Δ*flv3* deletion strains (Figure 4F) our results strongly argue in favor of Fd instead of NADPH as the primary electron donor to Flv1/3.

Deficiency of NDH-1L, in contrast, decreased the cells' ability to keep P700 and Fd oxidized under high irradiance in fast time scale (~50–200 ms) during dark-to-light transition (Figure 5C). The fast timescale may derive from formation of PSI-NDH-1 supercomplexes (Gao et al., 2016) where P700 can be oxidized rapidly upon onset of illumination. It has been shown that formation of the NDH-1-PSI supercomplex is important to keep PSI functional under various stress conditions (Zhao et al. 2017). NDH-1L-deficiency also caused slightly elevated acceptor side limitation of PSI under low irradiance (Figure 3A), which was likely due to lack of NADPH oxidation during the LL phases of fluctuating light (Figure 4C), supporting an important role for NDH-1L under low light, as has been suggested previously for chloroplastic NDH in angiosperms (Yamori et al., 2011; Yamori et al., 2015) and bryophytes (Ueda et al., 2012)). Delayed activation of CBC in Δ*d1d2* did not result in inability to oxidize PSI (Figure 3B and Figure 5C) likely due to significant enhancement of FDP-mediated O_2 photoreduction (Figure 2C), which provided an enlarged electron sink for the photosynthetic electron transfer chain. It has not escaped our notice that an opposite order of causation is also possible, whereby the excessive funneling of photosynthetic electrons to O_2 would cause the delay in induction of CO_2 fixation in Δ*d1d2*. However, the observation that NADPH accumulates similarly to WT at the onset of illumination in Δ*d1d2,* and rather the consumption of NADPH during transitions from HL to LL is impaired (Figure 4C), suggests that the availability of reductant for the CBC is not the limiting factor. Nor is it likely CO_2, as CCM is functioning as in WT (Figure 2C), or ATP, as ATP synthase activity was even higher than in WT in Δ*d1d2* (Figure 5F). Nevertheless, simultaneous deficiency of Flv1/3 in addition to NDH-1L (in Δ*flv3 d1d2* triple mutant), with the effect of diminishing the direction of photosynthetic electrons to O_2 photoreduction, mostly rescued the delay in CO_2 fixation seen in Δ*d1d2* (Figure 2). Transient O_2 photoreduction at a low rate was still observed in Δ*flv3 d1d2* during dark-to-HL transitions (Figure 2D), possibly mediated by the thylakoid terminal oxidases Cox and Cyd (Ermakova et al., 2016) or by photorespiration (Allahverdiyeva et al., 2011). However, the triple mutants suffered from more severe inability to oxidize PSI than Δ*flv3* during sudden increases in irradiance (Figure 3). These observations suggest that in addition Flv1/3, also NDH-1L has a role in contributing to oxidation of PSI during changes in light conditions or carbon availability. Upon deficiency of NDH-1L (in Δ*d1d2*), cells prioritize protection of PSI over efficient carbon fixation by upregulating the Mehler-like reaction via an unknown mechanism. The triple mutants cannot do this, leading to timely

induction of carbon fixation at the high cost of inability to oxidize PSI (Figure 3A and 3) or Fd (Figure 5D). This results in loss of PSI (Figure 6), possibly due to photodamage to its FeS clusters (Tiwari et al., 2016; Shimakawa et al., 2016).

On the mechanism of NDH-1-mediated oxidation of PSI

Contribution of NDH-1 to oxidation of PSI during sudden increases in light intensity is not unprecedented. In angiosperm plants, where FDPs have been lost during evolution (Ilik et al., 2017), mutants lacking the NDH complex show a delay in oxidation of PSI during increases in light intensity (Nikkanen et al., 2018; Shimakawa and Miyake, 2018a). By definition, canonical CET cannot directly increase the relative proportion of oxidized P700 pairs, as electrons from the acceptor side of PSI are shunted back to the intersystem electron transfer chain. However, NDH-1 may enhance PSI oxidation by at least three alternative, but mutually non-exclusive mechanisms.

i) NDH-1-mediated CET is coupled to translocation of protons from cytosol to the thylakoid lumen with a $2H^+/e^-$ stoichiometry (Strand et al., 2017; Saura and Kaila, 2019). It will therefore contribute to buildup of ΔpH, which limits electron transfer to PSI by inhibiting PQH_2 oxidation at Cyt *b6f* (Shimakawa and Miyake, 2018b) and drives ATP synthesis to accommodate the needs of the CBC, increasing its electron sink capacity. As the Mehler-like reaction also contributes to buildup of ΔpH by consuming H^+ on the cytosolic side of the thylakoid membrane and by supporting linear electron flow (Figure 5), (Allahverdiyeva et al., 2013), enhanced FDP activity in Δ*d1d2* (Figure 2C) partly compensates for the lack of NDH-1L in respect to generation of proton flux (Figure 5G). However, this fails to explain the exacerbated impairment of P700 and Fd oxidation in Δ*flv3 d1d2* in comparison to Δ*flv3* (Figure 3 and Figure 5) because in the triple mutant *pmf* was not lower than in Δ*flv3* (Figure 5E). Adequate *pmf* is maintained however at the expense of ATP synthase activity (Figure 5F), and it is likely that diminished ATP production contributes to the increased acceptor side limitation of PSI in Δ*flv3 d1d2* (Figure 3A). NDH-1L could therefore contribute to P700 oxidation by enhancing cytosolic sink capacity by providing a more suitable ATP:NADPH ratio for the CBC. Adjustment of the ATP:NADPH ratio closer to the theoretically optimal 3:2 has long been considered a fundamental reason for the existence of CET (Kramer et al., 2004; Yamori and Shikanai, 2016).

ii) NDH-1-mediated respiratory electron transfer, *i.e.* coupling of PQ reduction to O_2 reduction by thylakoid RTOs (*i.e.* Cyd and Cox) would also contribute to oxidation of PSI by

relieving electron pressure in the intersystem chain (Ermakova et al., 2016), as well as further contribute to ΔpH by consuming H^+ on the cytosolic side of thylakoids (Cyd) and pumping protons to the lumen (Cox) (Branden et al., 2006). Interestingly, Liu and colleagues (2012) have shown that the subcellular localization of NDH-1 complexes is dependent on the redox state of the PQ pool. An oxidized PQ pool causes NDH-1 to accumulate at specific clusters in thylakoid membranes where it would be more likely to transfer electrons (via the PQ pool) to a terminal oxidase. A reduced PQ pool, in turn, results in a more even distribution of NDH-1 within thylakoids (Liu et al., 2012).

iii) Thirdly, NDH-1 has been predicted, albeit not yet experimentally shown in photosynthetic organisms, to be able to function in reverse: to oxidize PQH_2 driven by concomitant release of protons from the thylakoid lumen (Strand et al., 2017). Such reverse activity would constitute a 'pseudo-linear' electron transfer pathway that would bypass PSI and thereby prevent its over-reduction. This could occur in conditions where the PQ pool is reduced, *pmf* is high, and the Fd pool is oxidized (Strand et al., 2017). Such conditions likely exist transiently during dark-to-light and LL-to-HL transitions (Figures 4 and 5) (Strand et al., 2019), and accordingly, fast re-reduction of $P700^+$ already after 50 ms was observed in Δ*d1d2* and Δ*flv3 d1d2* during dark-to-HL transitions (Figure 5C). As supported by the impaired ability to oxidize Fd in absence of Flv1/3 (Figure 5), the presence of Flv1/3-catalyzed Mehler-like reaction would likely be essential in this model in order to maintain the Fd pool in a sufficiently oxidized state to provide electron acceptors for reverse-functioning NDH-1. It is noteworthy, however, that NDH-1 reverse activity would also have the effect of lowering ΔpH, thereby relieving photosynthetic control at Cyt *b*6*f*. This could counteract the effect of any reverse NDH-1 activity by increasing electron flow to PSI.

Hypothetical mechanisms for coordination of Flv1/3 and NDH-1L activities are shown in Figure 7. An interesting question that remains to be answered in future studies pertains to whether the NdhD1 and NdhD2 isoforms have distinct physiological functions. NDH-1L and NDH-1L´ could have differing propensities for functioning in CET-mode, reverse-mode, or respiration-mode, as discussed above, depending on *pmf* and redox states of the PQ and Fd pools.

Inability to induce a strong CCM network contributes to lethality upon shifts to air [CO_2] / high irradiance in cells deficient in both Flv1/3 and NDH-1L

Interestingly, the change in growth conditions was lethal to the Δ*flv1d1d2* and Δ*flv3d1d2* mutants only when they underwent a decrease in [CO_2] coupled to increase in irradiance (Figure 1D). For instance, when shifted from air [CO_2] / GL to air [CO_2] / HL, the mutants grew similarly to WT (Figure 1C). This difference may depend on low C_i-induced expression of genes related to CCMs. SbtA and NdhD3 are high-affinity CCMs proteins, and their expression is strongly induced under low [CO_2] in WT cells (Shibata et al., 2002; Zhang et al., 2004). SbtA functions as a HCO_3^- / Na^+ symporter on the plasma membrane, while NdhD3 is part of the NDH-1MS complex on thylakoids specializing in C_i uptake (Ohkawa et al., 2000; Shibata et al., 2001). Considering that a large Ci flux involved in the operation of CCM largely contributes to dissipation of excess light energy (Burnap et al. 2015), its involvement in photoprotection is obvious (Xu et al. 2008). Despite the low induction level of the CCM proteins NdhD3 and SbtA, the triple mutants (Figure 6) survive under standard growth conditions (air [CO_2] / 50 μmol photons $m^{-2}s^{-1}$) (Figures 1B and 2D). Upon shifts to air [CO_2] / HL, however, a low amount of CCM depending on NdhD3 and SbtA (Figure 6C) fails to dissipate excess energy, thus resulting in photodamage and lethality of those conditions. After extended time to acclimate to air [CO_2], NdhD3 accumulated at WT level but SbtA content remained very low (Figure 6B), emphasizing the importance of NDH-1MS for functionality of the CCM. The regulatory mechanisms controlling the inability of the triple mutants to induce CCM proteins is unclear and remains to be elucidated in further studies. However, accumulation of NdhD3 and in particular SbtA have been reported to increase in more alkaline pH of 8.2 in the M55 mutant (lacking any NDH-1 complexes) (Zhang et al., 2004), suggesting that lowered cytosolic pH may affect the accumulation of NdhD3 and SbtA in the triple mutants. It is important to note however, that Flv1/3 and NDH-1MS cooperation is not crucial for cell metabolism, since the Δ*flv1 d3d4* and Δ*flv3 d3d4* mutant cells do not show clear growth phenotypes (Figure S1A-B).

In the current study we have shown that Flv1/3 and NDH-1 function cooperatively to maintain redox balance between the PETC and cytosolic carbon assimilation upon sudden changes in light intensity and/or carbon availability. It is likely that both pathways receive electrons primarily from Fd, which enables coordinated regulation of their activities. Cooperation of Flv1/3 and NDH-1 has an essential photoprotective role during shifts to HL / air [CO_2], contributing to efficient oxidation of PSI, buildup of *pmf*, and induction of expression of low [C_i]-specific CCM-related genes. Finally, it is worth noting that simultaneous removal of Flv1/3 and NDH-1L as competitive electron

sinks downstream of PSI may be a useful biotechnological tool for maximizing direction of photosynthetic electrons to desired pathways under controlled environmental conditions (McCormick et al., 2013; Thiel et al., 2019; Jokel et al., 2019). Furthermore, our findings about functional interplay between FDPs and NDH-1 will be highly relevant in projects aiming to enhance crop productivity via introduction of exogenous FDPs to higher plants (Yamamoto et al., 2016; Gómez et al., 2018).

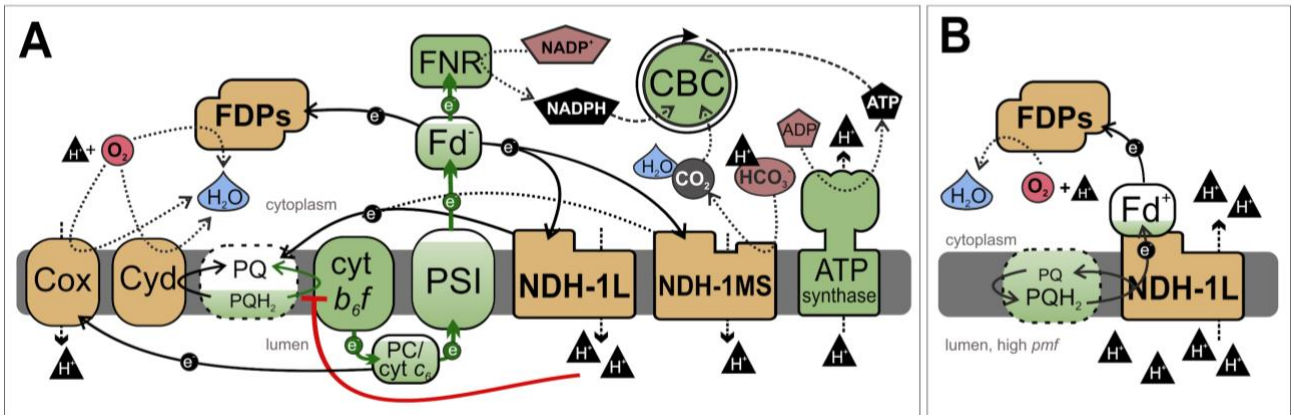

Figure 7. Schematic models for the coordination of the activities of FDPs and NDH-1 in preventing over-reduction of PSI. (A) In conditions where the Fd pool is higly reduced and the PQ pool is not, NDH-1L transfers electrons from Fd to the PQ pool, coupled to O_2 reduction by thylakoid-localised RTOs. NDH-1L pumps $2H^+/e^-$ into the lumen while FDPs and RTOs consume H^+ when reducing O_2 to H_2O on the cytosolic side of thylakoids. This increases transthylakoid *pmf*, which in turn drives ATP synthesis as well as inhibits PQH_2 oxidation at Cyt b_6f, thereby preventing excessive electron supply to PSI. Carbonic anhydrase activity of NDH1-MS converts HCO_3^- to CO_2, consuming H^+ in the cytosol, likely also coupled to translocation of H^+ to the lumen, further increasing *pmf*. Increased availability of CO_2 and ATP/NADPH ratio enhances the electron sink capacity of the CBC on the acceptor side of the PETC. **(B)** If the PQ pool is highly reduced, Fd pool is oxidized, and *pmf* is high, NDH-1L could hypothetically function in reverse, transferring electrons from PQH_2 to Fd^+, powered by release of $2H^+/e^-$ from the lumen. A strong Mehler-like reaction catalyzed by Flv1/3 would be required to maintain a sufficient pool of oxidized Fd, with Flv1/3 likely accepting electron directly from Fd^-. Most components depicted in (A) are omitted from (B) to enhance clarity, not to suggest their absence. Extent of the colour fill for PQ/PQH_2 and Fd depict level of reduction.

METHODS

Strains and culture conditions

In the current study we used the glucose-tolerant WT strain *Synechocystis* sp. PCC 6803 (Williams, 1988), previously described single mutant strains Δ*flv1* and Δ*flv3* (Helman et al., 2003), double mutant Δ*d1d2 and* Δ*d3d4* (Ohkawa et al., 2000), M55 Δ*flv3* (Figure S1C) as well as triple mutants strains Δ*flv1 d1d2,* Δ*flv3 d1d2*, Δ*flv2 d1d2*, Δ*flv1 d3d4, and* Δ*flv3 d3d4* which are described on the CyanoMutants website (http://www.kazusa.or. jp/cyano/mutants/) (Nakamura et al., 1999). Pre-experimental cultures were always grown in 30 ml batches of BG-11 medium (Williams, 1988) pH 7.5 in 3% [CO_2] at 30$_o$C under continuous white light of 50 µmol photons $m^{-2}s^{-1}$ (GL) with agitation. Mutant pre-cultures were supplemented with the appropriate antibiotics. At the logarithmic growth phase, cells were harvested and re-suspended in fresh BG-11 without antibiotics at OD_{750} of 0.1–0.2, as described in the appropriate figure legends. Cells were then shifted to air [CO_2] / 30$_o$C and illuminated continuously with white light of either 50 or 220 µmol photons $m^{-2}s^{-1}$, as described in the figure legends.

Gas exchange measurements

Exchange of $^{16}O_2$ (*m/z*=32), $^{18}O_2$ (*m/z*=36), CO_2 (*m/z*=44) was measured in vivo with membrane-inlet mass spectrometry (MIMS) as described in Mustila et al. (2016). Harvested cells were resuspended in fresh BG-11 pH 7.5 and adjusted to 10 µg Chl a ml^{-1}, and kept for one hour in air [CO_2] / 50 µmol photons $m^{-2}s^{-1}$. Prior to the measurements, cells were supplemented with $^{18}O_2$ at an equivalent concentration to $^{16}O_2$ and with 1.5 mM $NaHCO_3$. Cells were dark-adapted for 15 min, after which gas exchange was monitored over a 5 min illumination period of 500 µmol photons $m^{-2}s^{-1}$ of white actinic light (AL). The gas exchange rates were calculated according to Beckmann et al., (2009).

Measurement of fluorescence and absorbance changes

Experimental cultures for all spectroscopic experiments were grown for four days in air [CO_2] / 50 µmol photons $m^{-2}s^{-1}$ at 30$_o$C in BG-11 pH 7.5. Chl *a* fluorescence and P700-oxido-reduction (875-830 nm absorbance difference) were simultaneously recorded (Figure 3) with the Dual-PAM 100 spectrometer (Walz, Effeltrich, Germany). Harvested cells were resuspended in fresh BG-11 pH 7.5 and adjusted to 10 µg Chl a ml^{-1}, and kept for one hour in air [CO_2] / 50 µmol photons $m^{-2}s^{-1}$ and

dark-adapted for 10 min before being subjected to fluctuating light regime alternating between 1 min periods of 25 and 530 µmol photons $m^{-2}s^{-1}$ of red AL. Saturating pulses (500 ms of 5000 µmol photons $m^{-2}s^{-1}$) were administered at 15 s intervals. Photosynthetic parameters were calculated as follows: $Y(NA)=(P_m-P_m')/P_m$; $Y(ND)=P/P_m$; $Y(I)=1-Y(ND)-Y(NA)$ (Klughammer and Schreiber, 2008); $Y(II)=(F_m'-F)/F_m'$ (Genty et al., 1989).

A Dual-Klas NIR 100 spectrometer (Walz) was used to measure absorbance difference changes at 780–800 nm, 820–870 nm, 840–965 nm and 870–965 nm, from which PC, P700, and Fd redox changes (Figure 5) were deconvoluted based on differential model plots (DMPs) for PC, P700, and Fd (Klughammer and Schreiber, 2016; Schreiber, 2017; Setif et al., 2019). In WT *Synechocystis*, very fast re-oxidation of Fd upon illumination impedes measurement of model spectra. To circumvent this issue, we measured the DMPs from Δ*flv3 d1d2* cells where P700 oxidation was severely delayed in comparison to WT (Figure 3B). The DMPs (Figure S3) were measured using standard scripts provided with the instrument software. Harvested cells were adjusted to 10 µg Chl a ml^{-1} with fresh BG-11 pH 7.5, and kept for one hour in air [CO_2] / 50 µmol photons $m^{-2}s^{-1}$ and dark-adapted for 30 min before illumination for 30 s with 503 µmol photons $m^{-2}s^{-1}$ of red AL. It is noteworthy that cytochrome c_6 and (F_AF_B) redox changes likely contribute to the PC and Fd signals, respectively (Setif et al., 2019).

NADPH fluorescence changes between 420 and 580 nm, induced by excitation at 365 nm, were measured simultaneously with Chl a fluorescence with the Dual-PAM 100 and its 9-AA/NADPH accessory module (Walz) (Schreiber and Klughammer, 2009; Kauny and Setif, 2014). Experimental samples were prepared as above and [Chl] was adjusted to 5 µg ml^{-1}. Cells were dark-adapted for 10 min and subjected to the same fluctuating light regime as in Figure 3, but without saturating pulses.

Electrochromic shift (ECS) was measured as absorbance difference between 500 and 480 nm (Viola et al., 2019). Absorbance changes were measured from dark-adapted cell suspensions with a JTS-10 spectrometer (BioLogic, Seyssinet-Pariset, France) using 500 and 480 nm CWL 50mm 10nm FWHM bandpass filters (Edmund Optics, Barrington, NJ, USA) and BG39 filters (Schott, Mainz, Germany) protecting the light detectors from scattering effects. Absorbance changes induced by measuring light only were subtracted from changes under ML + AL. ECS values were normalized to ECS change induced by a single turnover saturating flash provided by a XST-103 xenon lamp (Walz). Experimental samples were prepared as above and [Chl] was adjusted to 7.5 µg ml^{-1}, and illuminated with green AL of 500 µmol photons $m^{-2}s^{-1}$ for 1s or 60 s interspersed with 500ms dark

intervals at 2, 7.5, 18, 30, and 45 s. *Pmf* was calculated as the extent of ECS decrease at the dark intervals. Thylakoid conductivity (gH+) was calculated as the inverse of the time constant of a first-order fit to ECS relaxation kinetics during a dark interval, and proton flux (vH+) as *pmf* x gH+ (Cruz. et al., 2005).

77K fluorescence emission spectra were measured with a QE Pro spectrophotometer (Ocean Optics, Dunedin, FL, USA). Cells were harvested and [Chl *a*] was adjusted to 7.5 µg ml^{-1} with fresh BG-11 pH 7.5. Cells were frozen in liquid N_2 and excited at 440 nm. Raw spectra were normalized to PSII-fluorescence peak at 685 nm.

Protein extraction and immunoblotting

Total protein extracts from cultures were isolated as previously described (Zhang et al., 2009), separated with SDS-PAGE on 12 % gels with 6M urea, and blotted on PVDF membranes. Membranes were probed with antibodies raised against D1, PsaB (Agrisera, Vännäs, Sweden, AS10 695), PetH (Kindly shared by H. Matthijs), OCP (kindly shared by D. Kirilovsky), SbtA (kindly shared by T. Ogawa), NdhD3 (Eurogentec, Liége, Belgium), Flv2 (Antiprot, Puchheim, Germany), sll0218 (MedProbe, Oslo, Norway), Flv4 (Antiprot), or Flv3 (Antiprot). Horseradish peroxidase – conjugated secondary antibody (GE Healthcare, Chicago, IL, USA) and Amersham ECL (GE Healthcare) were used for detection.

AUTHOR CONTRIBUTIONS

Y.A., and L.N. conceptualized the research; L.N., A.S.S., M.E., and Y.A. designed the research; M.E. conducted growth experiments; L.N. performed MIMS and spectrophotometric experiments; A.S.S. performed immunoblotting; all authors analyzed and interpret the data; L.N. and Y.A. wrote the article with the input from A.S.S and M.E.

ACKNOWLEDGEMENTS

We thank Prof. Teruo Ogawa for sharing the FDP and NDH-1 mutants and Dr. Henna Mustila for construction of the ΔM55 *flv3* strain. Dr. Duncan Fitzpatrick is thanked for expertise and assistance with MIMS. We also thank Dr. Pierre Setif and Dr. Gert Schansker for their expert advice on

measuring the DMPs for the Dual-Klas NIR spectrometer, and Prof. Jens Appel for critical reading of the manuscript. This work was supported by the Academy of Finland (project #315119 to Y.A. and the Finnish Center of Excellence, project #307335), the Nordforsk Nordic Center of Excellence 'NordAqua' (#82845) and SFB480- Germany. We declare no conflicts of interest.

REFERENCES

Alboresi A., Storti M., Cendron L., and Morosinotto T. (2019). Role and regulation of class-C flavodiiron proteins in photosynthetic organisms. Biochem. J. **476,** 2487-2498, doi/10.1042/BCJ20180648.

Allahverdiyeva Y., Ermakova M., Eisenhut M., Zhang P., Richaud P., Hagemann M., Cournac L., and Aro E. (2011). Interplay between Flavodiiron Proteins and Photorespiration in Synechocystis sp. PCC 6803. J. Biol. Chem. **286,** 24007-24014, doi/10.1074/jbc.M111.223289.

Allahverdiyeva Y., Mustila H., Ermakova M., Bersanini L., Richaud P., Ajlani G., Battchikova N., Cournac L., and Aro E. (2013). Flavodiiron proteins Flv1 and Flv3 enable cyanobacterial growth and photosynthesis under fluctuating light. Proc. Natl. Acad. Sci. U. S. A. **110,** 4111-4116, doi/10.1073/pnas.1221194110.

Allahverdiyeva Y., Suorsa M., Tikkanen M., and Aro E. (2015). Photoprotection of photosystems in fluctuating light intensities. J. Exp. Bot. **66,** 2427-2436, doi/10.1093/jxb/eru463.

Allakhverdiev S.I. and Murata N. (2004). Environmental stress inhibits the synthesis de novo of proteins involved in the photodamage-repair cycle of Photosystem II in Synechocystis sp PCC 6803. Biochim. Biophys. Acta Bioenerg. **1657,** 23-32, doi/10.1016/j.bbabio.2004.03.003.

Beckmann K., Messinger J., Badger M.R., Wydrzynski T., and Hillier W. (2009). On-line mass spectrometry: membrane inlet sampling. Photosynth. Res. **102**, 511-522. doi/10.1007/s11120-009-9474-7.

Bernat G., Appel J., Ogawa T., and Rögner M. (2011). Distinct Roles of Multiple NDH-1 Complexes in the Cyanobacterial Electron Transport Network as Revealed by Kinetic Analysis of P700(+) Reduction in Various ndh-Deficient Mutants of Synechocystis sp. Strain PCC6803. J. Bacteriol. **193,** 292-295, doi/10.1128/JB.00984-10.

Brändén G., Gennis R.B., and Brzezinski P. (2006). Transmembrane proton translocation by cytochrome c oxidase. Biochim. Biophys. Acta **1757,** 1052-1063, doi/10.1016/j.bbabio.2006.05.020.

Brown K.A., Guo Z., Tokmina-Lukaszewska M., Scott L.W., Lubner C.E., Smolinski S., Mulder D.W., Bothner B., and King P.W. (2019). The oxygen reduction reaction catalyzed by Synechocystis sp. PCC 6803 flavodiiron proteins. Sustain. Energy Fuels **3,** 3191-3200, doi/10.1039/c9se00523d.

Bulychev A.A., Cherkashin A.A., Muronets E.M., and Elanskaya I.V. (2018). Photoinduction of electron transport on the acceptor side of PSI in Synechocystis PCC 6803 mutant deficient in flavodiiron proteins Flv1 and Flv3. Biochim. Biophys. Acta Bioenerg. **1859,** 1086-1095, doi/10.1016/j.bbabio.2018.06.012.

Burnap R.L., Hagemann M., and Kaplan A. (2015). Regulation of CO_2 concentrating mechanism in cyanobacteria. Life (Basel) **5**, 348-371.

Burnap R.L., Nambudiri R., and Holland S. (2013). Regulation of the carbon-concentrating mechanism in the cyanobacterium Synechocystis sp PCC6803 in response to changing light

intensity and inorganic carbon availability. Photosynthesis Res. **118,** 115-124, doi/10.1007/s11120-013-9912-4.

Chaux F., Burlacot A., Mekhalfi M., Auroy P., Blangy S., Richaud P., and Peltier G. (2017). Flavodiiron Proteins Promote Fast and Transient O-2 Photoreduction in Chlamydomonas(1[OPEN]). Plant Physiol. **174,** 1825-1836, doi/10.1104/pp.17.00421.

Cooley J.W. and Vermaas W. (2001). Succinate dehydrogenase and other respiratory pathways in thylakoid membranes of Synechocystis sp strain PCC 6803: Capacity comparisons and physiological function. J. Bacteriol. **183,** 4251-4258, doi/10.1128/JB.183.14.4251-4258.2001.

Cruz J.A., Avenson T.J., Kanazawa A., Takizawa K., Edwards G.E., and Kramer D.M. (2005). Plasticity in light reactions of photosynthesis for energy production and photoprotection. J. Exp. Bot. **56,** 395-406.

Dann M. and Leister D. (2019). Evidence that cyanobacterial Sll1217 functions analogously to PGRL1 in enhancing PGR5-dependent cyclic electron flow. Nat. Comm. **10,** 5299, doi/10.1038/s41467-019-13223-0.

Ermakova M., Huokko T., Richaud P., Bersanini L., Howe C.J., Lea-Smith D.J., Peltier G., and Allahverdiyeva Y. (2016). Distinguishing the Roles of Thylakoid Respiratory Terminal Oxidases in the Cyanobacterium Synechocystis sp PCC 6803. Plant Physiol. **171,** 1307-1319, doi/10.1104/pp.16.00479.

Gao F., Zhao J., Chen L., Battchikova N., Ran Z., Aro E.M., Ogawa T., and Ma W. (2016). The NDH-1L-PSI Supercomplex Is Important for Efficient Cyclic Electron Transport in cyanobacteria. Plant Physiol. **172,** 1451-1464, doi/10.1104/pp.16.00585.

Genty B., Briantais J.M., and Baker N.R. (1989). The Relationship between the Quantum Yield of Photosynthetic Electron-Transport and Quenching of Chlorophyll Fluorescence. Biochim. Biophys. Acta **990,** 87-92, doi/10.1016/S0304-4165(89)80016-9.

Gerotto C., Alboresi A., Meneghesso A., Jokel M., Suorsa M., Aro E., and Morosinotto T. (2016). Flavodiiron proteins act as safety valve for electrons in Physcomitrella patens. Proc. Natl. Acad. Sci. U. S. A. **113,** 12322-12327, doi/10.1073/pnas.1606685113.

Gómez R., Carrillo N., Morelli M.P., Tula S., Shahinnia F., Hajirezaei M.R., and Lodeyro A.F. (2018). Faster photosynthetic induction in tobacco by expressing cyanobacterial flavodiiron proteins in chloroplasts. Photosynth. Res. **146**, 129-136-

Han X., Sun N., Xu M., and Mi H. (2017). Co-ordination of NDH and Cup proteins in CO2 uptake in cyanobacterium Synechocystis sp PCC 6803. J. Exp. Bot. **68,** 3869-3877, doi/10.1093/jxb/erx129.

He Z., Zheng F., Wu Y., Li Q., Lv J., Fu P., and Mi H. (2015). NDH-1L interacts with ferredoxin via the subunit NdhS in Thermosynechococcus elongatus. Photosynthesis Res. **126,** 341-349, doi/10.1007/s11120-015-0090-4.

Helman Y., Tchernov D., Reinhold L., Shibata M., Ogawa T., Schwarz R., Ohad I., and Kaplan A. (2003). Genes encoding a-type flavoproteins are essential for photoreduction of O-2 in cyanobacteria. Curr. Biol. **13,** 230-235, doi/10.1016/S0960-9822(03)00046-0.

Ilik P., Pavlovic A., Kouril R., Alboresi A., Morosinotto T., Allahverdiyeva Y., Aro E., Yamamoto H., and Shikanai T. (2017). Alternative electron transport mediated by flavodiiron proteins is operational in organisms from cyanobacteria up to gymnosperms. New Phytol. **214,** 967-972, doi/10.1111/nph.14536.

Jokel M., Johnson X., Peltier G., Aro E., and Allahverdiyeva Y. (2018). Hunting the main player enabling Chlamydomonas reinhardtii growth under fluctuating light. Plant J. **94,** 822-835, doi/10.1111/tpj.13897.

Jokel M., Nagy V., Tóth S.Z., Kosourov S., and Allahverdiyeva Y. (2019). Elimination of the flavodiiron electron sink facilitates long-term H2 photoproduction in green algae. Biotechnol. Biofuels **12,** 280, doi/10.1186/s13068-019-1618-1.

Kaplan A. and Reinhold L. (1999). CO2 concentrating mechanisms in photosynthetic microorganisms. Annu. Rev. Plant Physiol. Plant Mol. Biol. **50,** 539-570, doi/10.1146/annurev.arplant.50.1.539.

Kauny J. and Setif P. (2014). NADPH fluorescence in the cyanobacterium Synechocystis sp PCC 6803: A versatile probe for in vivo measurements of rates, yields and pools. Biochim. Biophys. Acta Bioenerg. **1837,** 792-801, doi/10.1016/j.bbabio.2014.01.009.

Klughammer C. and Schreiber U. (2008). Saturation Pulse method for assessment of energy conversion in PSI. PAM Application Notes **1,** 11-14.

Klughammer C. and Schreiber U. (2016). Deconvolution of ferredoxin, plastocyanin, and P700 transmittance changes in intact leaves with a new type of kinetic LED array spectrophotometer. Photosynthesis Res. **128,** 195-214.

Kramer D.M., Avenson T.J., and Edwards G.E. (2004). Dynamic flexibility in the light reactions of photosynthesis governed by both electron and proton reactions. Trends Plant Sci. **9,** 349-357.

Laughlin T.G., Bayne A.N., Trempe J.F., Savage D.F., and Davies K.M. (2019) Structure of the complex I-like molecule NDH of oxygenic photosynthesis. Nature **566**, 411–414.

Liran O., Shemesh E., and Tchernov D. (2018). Investigation into the CO2 concentrating step rates within the carbon concentrating mechanism of Synechocystis sp PCC6803 at various pH and light intensities reveal novel mechanistic properties. Algal Res. **33,** 419-429, doi/10.1016/j.algal.2018.06.020.

Liu L., Bryan S.J., Huang F., Yu J., Nixon P.J., Rich P.R., and Mullineaux C.W. (2012). Control of electron transport routes through redox-regulated redistribution of respiratory complexes. Proc. Natl. Acad. Sci. U. S. A. **109,** 11431-11436, doi/10.1073/pnas.1120960109.

Ma W. and Ogawa T. (2015). Oxygenic Photosynthesis-specific Subunits of Cyanobacterial NADPH Dehydrogenases. IUBMB Life **67,** 3-8, doi/10.1002/iub.1341.

McCormick A.J., Bombelli P., Lea-Smith D.J., Bradley R.W., Scott A.M., Fisher A.C., Smith A.G., and Howe C.J. (2013). Hydrogen production through oxygenic photosynthesis using the cyanobacterium Synechocystis sp PCC 6803 in a bio-photoelectrolysis cell (BPE) system. Energy Environ. Sci. **6,** 2682-2690, doi/10.1039/c3ee40491a.

Mullineaux C.W. (2014). Co-existence of photosynthetic and respiratory activities in cyanobacterial thylakoid membranes. Biochim. Biophys. Acta Bioenerg. **1837,** 503-511, doi/10.1016/j.bbabio.2013.11.017.

Mustila H., Paananen P., Battchikova N., Santana-Sanchez A., Muth-Pawlak D., Hagemann M., Aro E., and Allahverdiyeva Y. (2016). The Flavodiiron Protein Flv3 Functions as a Homo-Oligomer During Stress Acclimation and is Distinct from the Flv1/Flv3 Hetero-Oligomer Specific to the O-2 Photoreduction Pathway. Plant Cell Physiol. **57,** 1468-1483, doi/10.1093/pcp/pcw047.

Nakamura Y., Kaneko T., Miyajima N., and Tabata S. (1999). Extension of CyanoBase. CyanoMutants: repository of mutant information on Synechocystis sp strain PCC6803. Nucleic Acids Res. **27,** 66-68, doi/10.1093/nar/27.1.66.

Nikkanen L., Toivola J., Trotta A., Guinea Diaz M., Tikkanen M., Aro E., and Rintamäki E. (2018). Regulation of cyclic electron flow by chloroplast NADPH-dependent thioredoxin system. Plant Direct **2,** 1-24.

Ohkawa H., Pakrasi H.B., and Ogawa T. (2000). Two types of functionally distinct NAD(P)H dehydrogenases in Synechocystis sp strain PCC6803. J. Biol. Chem. **275,** 31630-31634, doi/10.1074/jbc.M003706200.

Peltier G., Aro E., and Shikanai T. (2016). NDH-1 and NDH-2 Plastoquinone Reductases in Oxygenic Photosynthesis. Annual Review of Plant Biology, Annu. Rev. Plant Biol. **67,** 55-80.

Santana-Sanchez A., Solymosi D., Mustila H., Bersanini L., Aro E., and Allahverdiyeva Y. (2019). Flavodiiron proteins 1-to-4 function in versatile combinations in O-2 photoreduction in cyanobacteria. eLife **8,** e45766, doi/10.7554/eLife.45766.

Saura P. and Kaila V.R.I. (2019). Molecular dynamics and structural models of the cyanobacterial NDH-1 complex. Biochim. Biophys. Acta Bioenerg. **1860,** 201-208, doi/10.1016/j.bbabio.2018.11.010.

Schreiber U. and Klughammer C. (2009). New NADPH/9-AA module for the DUAL-PAM-100: Description, operation and examples of application. PAM Application Notes **2,** 1-13.

Schreiber U. (2017). Redox changes of ferredoxin, P700, and plastocyanin measured simultaneously in intact leaves. Photosynthesis Res. **134,** 343-360.

Schuller J.M., Birrell J.A., Tanaka H., Konuma T., Wulflhorst H., Cox N., Schuller S.K., Thiemann J., Lubitz W., Setif P., Ikegamis T., Engel B.D., Kurisu G., and Nowaczyk M.M. (2019). Structural adaptations of photosynthetic complex I enable ferredoxin-dependent electron transfer. Science **363,** 257-260, doi/10.1126/science.aau3613.

Setif P., Boussac A., and Krieger-Liszkay A. (2019). Near-infrared in vitro measurements of photosystem I cofactors and electron-transfer partners with a recently developed spectrophotometer. Photosynth Res., doi/10.1007/s11120-019-00665-2.

Shibata M., Ohkawa H., Kaneko T., Fukuzawa H., Tabata S., Kaplan A., and Ogawa T. (2001). Distinct constitutive and low-CO2-induced CO2 uptake systems in cyanobacteria: Genes involved and their phylogenetic relationship with homologous genes in other organisms. Proc. Natl. Acad. Sci. U. S. A. **98,** 11789-11794, doi/10.1073/pnas.191258298.

Shibata M., Katoh H., Sonoda M., Ohkawa H., Shimoyama M., Fukuzawa H., Kaplan A., and Ogawa T. (2002). Genes essential to sodium-dependent bicarbonate transport in cyanobacteria - Function and phylogenetic analysis. J. Biol. Chem. **277,** 18658-18664, doi/10.1074/jbc.M112468200.

Shimakawa G., Shaku K., and Miyake C. (2016). Oxidation of P700 in Photosystem I Is Essential for the Growth of Cyanobacteria. Plant Physiol. **172,** 1443-1450, doi/10.1104/pp.16.01227.

Shimakawa G. and Miyake C. (2018a). Changing frequency of fluctuating light reveals the molecular mechanism for P700 oxidation in plant leaves. Plant Direct **2,** e00073.

Shimakawa G. and Miyake C. (2018b). Oxidation of P700 Ensures Robust Photosynthesis. Front. Plant Sci. **9,** 1617, doi/10.3389/fpls.2018.01617.

Strand D., D'Andrea L., and Bock R. (2019). The plastid NAD(P)H dehydrogenase-like complex: structure, function and evolutionary dynamics. Biochem. J. **476,** 2743-2756, doi/10.1042/BCJ20190365.

Strand D.D., Fisher N., and Kramer D.M. (2017). The higher plant plastid NAD(P)H dehydrogenase-like complex (NDH) is a high efficiency proton pump that increases ATP production by cyclic electron flow. J. Biol. Chem. **292,** 11850-11860.

Thiel K., Patrikainen P., Nagy C., Fitzpatrick D., Pope N., Aro E.M., and Kallio P. (2019). Redirecting photosynthetic electron flux in the cyanobacterium Synechocystis sp. PCC 6803 by the deletion of flavodiiron protein Flv3. Microb. Cell. Fact. **18,** 189-2, doi/10.1186/s12934-019-1238-2

Tikkanen M., Mekala N.R., and Aro E. (2014). Photosystem II photoinhibition-repair cycle protects Photosystem I from irreversible damage. Biochim. Biophys. Acta **1837,** 210-215, doi/10.1016/j.bbabio.2013.10.001.

Tiwari A., Mamedov F., Grieco M., Suorsa M., Jajoo A., Styring S., Tikkanen M., and Aro E. (2016). Photodamage of iron-sulphur clusters in photosystem I induces non-photochemical energy dissipation. Nat. Plants **2,** 16035.

Ueda M., Kuniyoshi T., Yamamoto H., Sugimoto K., Ishizaki K., Kohchi T., Nishimura Y., and Shikanai T. (2012). Composition and physiological function of the chloroplast NADH dehydrogenase-like complex in Marchantia polymorpha. Plant J. **72,** 683-693, doi/10.1111/j.1365-313X.2012.05115.x.

Vicente J.B., Gomes C.M., Wasserfallen A., and Teixeira M. (2002). Module fusion in an A-type flavoprotein from the cyanobacterium Synechocystis condenses a multiple-component

pathway in a single polypeptide chain. Biochem. Biophys. Res. Commun. **294,** 82-87, doi/10.1016/S0006-291X(02)00434-5.

Viola S., Bailleul B., Yu J., Nixon P., Selles J., Joliot P., and Wollman F. (2019). Probing the electric field across thylakoid membranes in cyanobacteria. Proc. Natl. Acad. Sci. U. S. A. **116,** 21900-21906, doi/10.1073/pnas.1913099116.

Williams J.G.K. (1988). Construction of Specific Mutations in Photosystem-Ii Photosynthetic Reaction Center by Genetic-Engineering Methods in Synechocystis-6803. Meth. Enzymol. **167,** 766-778.

Xu M., Bernát G., Singh A., Mi H., Rögner M., Pakrasi H.B., and Ogawa T. (2008). Properties of mutants of Synechocystis sp. strain 6803 lacking inorganic carbon sequestration systems. Plant Cell Physiol. **49**, 1672-1677, doi/10.1093/pcp/pcn139

Yamamoto H., Takahashi S., Badger M.R., and Shikanai T. (2016) Artificial remodelling of alternative electron flow by flavodiiron proteins in Arabidopsis. Nat. Plants **2**, 16012 doi/ 10.1038/nplants.2016.12.

Yamori W., Sakata N., Suzuki Y., Shikanai T., and Makino A. (2011). Cyclic electron flow around photosystem I via chloroplast NAD(P)H dehydrogenase (NDH) complex performs a significant physiological role during photosynthesis and plant growth at low temperature in rice. Plant J. **68,** 966-976.

Yamori W., Shikanai T., and Makino A. (2015). Photosystem I cyclic electron flow via chloroplast NADH dehydrogenase-like complex performs a physiological role for photosynthesis at low light (vol 5, 13908, 2015). Sci. Rep. **5,** 15593.

Yamori W. and Shikanai T. (2016). Physiological Functions of Cyclic Electron Transport Around Photosystem I in Sustaining Photosynthesis and Plant Growth. Annu. Rev. Plant Biol. **67,** 81-106.

Yeremenko N., Jeanjean R., Prommeenate P., Krasikov V., Nixon P.J., Vermaas W., Havaux M., and Matthijs H. (2005). Open reading frame ssr2016 is required for antimycin A-sensitive photosystem I-driven cyclic electron flow in the cyanobacterium Synechocystis sp PCC 6803. Plant Cell Physiol. **46,** 1433-1436, doi/10.1093/pcp/pci147.

Zhang P., Battchikova N., Jansen T., Appel J., Ogawa T., and Aro E.M. (2004). Expression and functional roles of the two distinct NDH-1 complexes and the carbon acquisition complex NdhD3/NdhF3/CupA/Sll1735 in Synechocystis sp PCC 6803. Plant Cell **16,** 3326-3340, doi/10.1105/tpc.104.026526.

Zhang P., Allahverdiyeva Y., Eisenhut M., and Aro E. (2009). Flavodiiron Proteins in Oxygenic Photosynthetic Organisms: Photoprotection of Photosystem II by Flv2 and Flv4 in Synechocystis sp PCC 6803. PLoS One **4,** e5331, doi/10.1371/journal.pone.0005331.

Zhao J., Gao F., Fan DY., Chow WS., Ma W. (2017) NDH-1 Is Important for Photosystem I function of *Synechocystis* sp. strain PCC 6803 under environmental stress conditions. Front. Plant Sci. **8**: 2183, doi/10.3389/fpls.2017.02183.

FIGURE LEGENDS

Figure 1. Growth of WT and mutant strains in different experimental conditions. All experimental cultures were started from pre-cultures in BG-11 pH 7.5 adjusted to OD_{750}=0.1. **(A)** Cells were pre-cultivated under 3% [CO_2] and 50 µmol photons $m^{-2}s^{-1}$, adjusted to OD_{750}=0.1 and grown in the same conditions. **(B)** Cells were pre-cultivated under 3% [CO_2] and 50 µmol photons $m^{-2}s^{-1}$ and shifted to air [CO_2] and 50 µmol photons $m^{-2}s^{-1}$. **(C)** Cells were pre-cultivated under air

[CO_2] and 50 µmol photons $m^{-2}s^{-1}$ and shifted to air [CO_2] and 220 µmol photons $m^{-2}s^{-1}$. **(D)** Cells were pre-cultivated under 3% [CO_2] and 50 µmol photons $m^{-2}s^{-1}$ and shifted to air [CO_2] and 220 µmol photons $m^{-2}s^{-1}$. The values presented in A–D are means of three independent biological replicates ±SE. **(E)** Growth of WT and mutant cells on BG-11 (pH 7.5) agar plates. Cells grown under 3% [CO_2] / 50 µmol photons $m^{-2}s^{-1}$ were harvested and spotted on BG-11 agar plates in series of ten-fold dilutions from cells at OD_{750}=1, and incubated under air [CO_2] and 50 µmol photons $m^{-2}s^{-1}$ and air [CO_2] and 220 µmol photons $m^{-2}s^{-1}$ for 7 days. See also Figure S1.

Figure 2. O_2 and CO_2 exchange rates in WT and mutant strains. Cells were grown in air [CO_2] / 50 µmol photons $m^{-2}s^{-1}$ for 4 days in BG-11 pH 7.5, after which the cells were harvested and Chl *a* concentration adjusted to 10 µg ml^{-1} with fresh BG-11. Cells were dark-adapted for 15 min, and gas exchange was monitored by membrane inlet mass spectrometry (MIMS) over a 5 min illumination period with 500 µmol photons $m^{-2}s^{-1}$ of white actinic light. . Prior to the measurements, samples were supplemented with $^{18}O_2$ at an equivalent concentration to $^{16}O_2$ to distinguish O_2 uptake from O_2 evolution, and with 1.5 mM $NaHCO_3$. The dashed line in each panel indicates the compensation point of CO_2 fixation (uptake rate equals respiratory rate). The experiment was repeated with three independent biological replicates, of which representative measurements are shown. See also Figure S2.

Figure 3. Photosynthetic parameters in WT and mutants strains in fluctuating light. (A) Acceptor side limitation of PSI, Y(NA), **(B)** donor side limitation of PSI, Y(ND), as well as **(C)** quantum yield of PSI, Y(I) were calculated from absorbance difference changes at 875-830 nm according to (Klughammer and Schreiber, 2008). Chl *a* fluorescence changes were measured simultaneously with PSI redox changes and used to calculate **(D)** quantum yield of PSII. Cells were grown in air [CO_2] / 50 µmol photons $m^{-2}s^{-1}$ for 4 days in BG-11 pH 7.5, after which the cells were harvested and Chl *a* concentration adjusted to 10 µg ml^{-1} with fresh BG-11. Cells were dark-adapted for 10 min, and then subjected to illumination with red actinic light whose intensity was alternating between 25 and 530 µmol photons $m^{-2}s^{-1}$ in 1 min periods. Saturating pulses (500 ms of 5000 µmol photons $m^{-2}s^{-1}$) were provided every 15 seconds. The values shown are averages from 3–4 independent biological replicates ±SE. See also Figure S2.

Figure 4. NADPH and Chl *a* fluorescence under fluctuating light in WT and mutant strains. WT **(A)**, Δ*flv3* **(B)**, Δ*d1d2* **(C)**, and Δ*flv3 d1d2* cells **(D)** were grown in air [CO_2] / 50 µmol photons $m^{-2}s^{-1}$ for 4 days in BG-11 pH 7.5, after which the cells were harvested and Chl a concentration adjusted to 5 µg ml^{-1} with fresh BG-11. Cells were dark-adapted for 10 min, and then subjected to

illumination with red actinic light alternating between 25 and 530 µmol photons $m^{-2}s^{-1}$ in 1 min periods. NADPH redox changes were monitored with the Dual-PAM 100 spectrometer and its 9-AA/NADPH accessory module by measuring fluorescence changes between 420 and 580 nm induced by excitation at 365 nm, as described by (Schreiber and Klughammer, 2009) and (Kauny and Setif, 2014). Chl *a* fluorescence was recorded simultaneously. **(E)** NADPH redox changes during illumination of dark-adapted cells with 530 µmol photons $m^{-2}s^{-1}$. Other experimental details are as in A-D. **(F)** shows a magnification of the first 2 s of illumination in (E). The values are normalized according to minimum and maximum fluorescence changes at the onset and cessation of illumination, respectively. The experiments were repeated with three independent biological replicates, of which representative measurements are shown. r.u. = relative units.

Figure 5. Redox changes of PC, P700, and Fd, and buildup of *pmf* during dark-to-HL transitions. WT **(A)**, Δ*flv3* **(B)**, Δ*d1d2* **(C)**, and Δ*flv3 d1d2* cells **(D)** were dark-adapted for 10 min, after which absorbance difference changes at 780–800 nm, 820–870 nm, 840–965 nm and 870–965 nm were measured with the Klas-NIR 100 spectrometer during 30 s illumination at 503 µmol photons $m^{-2}s^{-1}$ of red actinic light. The PC, P700, and Fd signals were deconvoluted from the absorbance difference changes using differential model plots (DMPs) determined for this study (Figure S3). The upper panels in A–D show magnifications of the first 1.5 seconds of illumination from the lower panels. The experiment was repeated with three independent biological replicates, of which representative traces are shown. See also Figure S3. **(E)** Buildup of *pmf* during transitions from dark to 500 µmol photons $m^{-2}s^{-1}$ of green actinic light. Absorbance difference between 500-480 nm (ECS) was measured with a JTS-10 spectrometer, and light-induced *pmf* was determined from the dark interval relaxation kinetics (DIRK) of the ECS signal. Means ±SEM from 3–4 independent experiments are shown. The small inset shows *pmf* values after 1s of illumination for a clearer view. **(F)** Conductivity of the thylakoid membrane (gH+) after one and 30 s of illumination as in (E). gH+ was determined as the inverse of the time constant of first-order post-illumination decay kinetics of the ECS signal. **(G)** Thylakoid proton flux (vH+), calculated as *pmf* vx gH+. **(H)** Representative traces of 500-480 nm absorbance differences used to determine the values in (E) and post-illumination ECS decay kinetics during a 500 ms dark interval after 30 s in light (lower panels). First-order fits are shown in green. Cells were grown in air [CO_2] / 50 µmol photons $m^{-2}s^{-1}$ for 4 days in BG-11 pH 7.5, after which cells were harvested and Chl *a* concentration adjusted to 10 µg ml^{-1} with fresh BG-11 for A–D and to 7.5 µg ml^{-1} for E–J.

Figure 6. Immunodetection of proteins related to photosynthesis and CCM and 77K fluorescence emission spectra in WT and mutant strains. Pre-cultures were first grown for 3 days in BG-11 pH 7.5 at 3% [CO_2] / 50 µmol photons $m^{-2}s^{-1}$ and then pelleted, resuspended in fresh BG-11 pH 7.5 at OD_{750}=0.15 and **(A)** incubated for 24 hours in air [CO_2] / 50 µmol photons $m^{-2}s^{-1}$, **(B)** grown for 4 days in air [CO_2] / 50 µmol photons $m^{-2}s^{-1}$, harvested, resuspended in BG-11 at OD_{750}=0.15 and then incubated for 24 hours in air [CO_2] / 220 µmol photons $m^{-2}s^{-1}$, **(C)** incubated for 24 hours in air [CO_2] / 220 µmol photons $m^{-2}s^{-1}$. Total protein extracts were separated by SDS-PAGE and probed with specific antibodies. The immunoblots shown are representative of 2–3 independent biological replicates. **(D)** 77K fluorescence emission spectra from intact WT and Δ*flv3 d1d2* cells grown for 4 days in air [CO_2] / 50 µmol photons $m^{-2}s^{-1}$. **(E)** After pre-growth at 3% [CO_2] / 50 µmol photons $m^{-2}s^{-1}$ cells were pelleted, resuspended in fresh BG-11 pH 7.5 at OD_{750}=0.15 and incubated for 24 hours in air [CO_2] / 220 µmol photons $m^{-2}s^{-1}$. The cells (D and E) were pelleted, adjusted to [Chl *a*] of 7.5 µg ml^{-1}, and excited with 440 nm light at 77K. The spectra were normalized to the PSII fluorescence peak at 685 nm.

Figure 7. Schematic models for the coordination of the activities of FDPs and NDH-1 in preventing over-reduction of PSI. (A) In conditions where the Fd pool is higly reduced and the PQ pool is not, NDH-1L transfers electrons from Fd to the PQ pool, coupled to O_2 reduction by thylakoid-localised RTOs. NDH-1L pumps $2H^+/e^-$ into the lumen while FDPs and RTOs consume H^+ when reducing O_2 to H_2O on the cytosolic side of thylakoids. This increases transthylakoid *pmf*, which in turn drives ATP synthesis as well as inhibits PQH_2 oxidation at Cyt b_6f, thereby preventing excessive electron supply to PSI. Carbonic anhydrase activity of NDH1-MS converts HCO_3^- to CO_2, consuming H^+ in the cytosol, likely also coupled to translocation of H^+ to the lumen, further increasing *pmf*. Increased availability of CO_2 and ATP/NADPH ratio enhances the electron sink capacity of the CBC on the acceptor side of the PETC. **(B)** If the PQ pool is highly reduced, Fd pool is oxidized, and *pmf* is high, NDH-1L could hypothetically function in reverse, transferring electrons from PQH_2 to Fd^+, powered by release of $2H^+/e^-$ from the lumen. A strong Mehler-like reaction catalyzed by Flv1/3 would be required to maintain a sufficient pool of oxidized Fd, with Flv1/3 likely accepting electron directly from Fd^-. Most components depicted in (A) are omitted from (B) to enhance clarity, not to suggest their absence. Extent of the colour fill for PQ/PQH_2 and Fd depict level of reduction.